Recruitment of inflammatory monocytes by senescent fibroblasts inhibits antigen-specific tissue immunity during human aging

Emma S Chambers[1,$,*], Milica Vukmanovic-Stejic[1*], Barbara B Shih[2], Hugh Trahair[1], Priya Subramanian[1], Oliver P Devine[1], James Glanville[3], Derek Gilroy[3], Malcolm Rustin[4], Tom C Freeman[2], Neil A Mabbott[2], and Arne N Akbar[1#]

1. Division of Infection and Immunity, University College London, WC1E 6EJ, U.K.
2. The Roslin Institute and Royal (Dick) School of Veterinary Studies, University of Edinburgh, Easter Bush, Midlothian, EH25 9RG, U.K.
3. Division of Medicine, University College London, WC1E 6EJ, U.K.
4. Department of Dermatology, Royal Free Hospital, London

* ESC and MVS contributed equally to this work.

$ Current address: Centre for Immunobiology, Blizard Institute, Queen Mary University of London, 4 Newark Street, London E1 2AT

Corresponding author:

Professor Arne N. Akbar, The Rayne Building, 5 University Street, Division of Infection and Immunity, University College London, London, WC1E 6EJ. United Kingdom.

E-mail: a.akbar@ucl.ac.uk

Tel: +44-203-108 2172

Short Title: Monocyte-derived PGE_2 inhibits cutaneous immunity

Summary Sentence: Prostaglandin E_2 produced by inflammatory monocytes inhibit skin T_{RM} function and antigen-specific immunity in older adults.

Abbreviations:

CBA – cytometric bead array

CRP - C reactive protein

COX2 – Cyclooxygenase 2

DC – Dendritic Cell

EP4 - Prostaglandin E2 receptor 4

LPS – Lipopolysaccharide

ILT - Immunoglobulin-like transcript

p38-MAPK - p38 mitogen-activated protein kinase

PD-L - Programme-death ligand

PGE_2 - Prostaglandin E2

PV – perivascular infiltrate

SASP - senescence associated secretory phenotype

TAF - telomere-associated DNA-damage

Tregs - T regulatory cells

T_{RM} - T resident-memory cells

VZV - Varicella Zoster Virus

Abstract:

We have previously shown that healthy older adults exhibit reduced cutaneous immune responses during a varicella zoster virus (VZV) antigen challenge that correlated with a non-specific inflammatory response to the injection itself.

Here we found that needle damage during intradermal injections in older adults led to an increase in the number of cutaneous senescent fibroblasts expressing CCL2, resulting in the local recruitment of inflammatory monocytes. These infiltrating monocytes secreted prostaglandin E2 (PGE_2) that inhibited resident memory T cell (T_{RM}) activation and proliferation. Pre-treatment of older subjects with a p38-MAPK inhibitor *in vivo* decreased CCL2 expression and inhibited monocyte recruitment and secretion of PGE_2. This coincided with an increased response to VZV antigen challenge in the skin.

Our results point to a series of molecular and cellular mechanisms that link cellular senescence, tissue damage, excessive inflammation and reduced immune responsiveness in human skin and demonstrate that tissue-specific immunity can be restored in older adults by the short-term inhibition of inflammatory responses.

Introduction:

Immunity decreases during ageing as demonstrated by the increased susceptibility to infections including pneumonia and influenza, re-activation of latent infections such as varicella zoster virus (VZV), decreased vaccine efficacy and increased incidence of cancer[1, 2, 3]. In addition, there is an increase in low grade systemic inflammation in older humans termed inflammageing, that is characterised by high serum levels of the inflammatory cytokines IL-6, IL-1β, TNFα and C reactive protein (CRP)[4]. This elevated expression of inflammatory proteins is a strong predictor for frailty and mortality[5, 6]. Mechanisms that contribute to inflammageing are multifactorial, and include increased numbers of senescent cells (which secrete many inflammatory proteins as part of the senescence associated secretory phenotype (SASP), increased gut permeability and subsequent lipopolysaccharide (LPS; a TLR4 ligand) exposure, expression of damage-associated molecular pattern molecules (DAMPs) and failure of immune resolution[7].

Cutaneous recall antigen challenge is often used as a measure of effective immunity. Older individuals have reduced responses to challenge with various recall antigens including tuberculin PPD, *Candida albicans* and varicella zoster virus (VZV) antigens [8, 9, 10, 11]. We showed previously that this decrease was a result of heightened inflammatory responses in the skin of older individuals during immune challenge and not from changes in antigen-specific circulating or skin resident-memory T cells (T_{RM})[12]. However, the mechanism by which inflammation inhibits antigen-specific immunity in the skin is unknown.

Here we show that when challenging old individuals in the skin with VZV antigens, the tissue damage caused by the injection of the VZV antigen itself induces senescent fibroblasts to recruit $CCR2^{+}CD14^{+}$ monocytes from the circulation. These infiltrating monocytes express cyclooxygenase 2 (COX2) and produce prostaglandin E2 (PGE_2) that inhibits T_{RM} activation and proliferation. Pre-treatment of older individuals with and oral p38 MAPK inhibitor inhibited monocyte recruitment and PGE_2 production during the immune response to VZV.

This resulted in a significantly enhanced VZV-specific mediated delayed type hypersensitivity responses associated with the activation and expansion of T cell numbers in the skin. These data identify a broad mechanism by which even mild tissue damage may induce inflammation in the tissues of older individuals that can inhibit immunity. An important consideration is whether the short-term blockade of inflammation would enhance the immune responses of older humans at early stages of (pathogen) infection where the infectious agent may induce damage and excessive inflammation that may retard subsequent immune responsiveness.

Results:

Inappropriate response to tissue damage in the skin during ageing

Old (≥65 years) and young (<40 years) individuals were recruited for this study, donor characteristics can be found in Supplementary Table 1. Although there were more females in the older adult group, there was no difference in response between the different genders within this group (Extended Figure 1A). Volunteers were injected intradermally with VZV skin test antigen in one arm (for the clinical score) and with saline (0.9% NaCl) in the other arm as a control. 5mm biopsies were collected from the injection sites 6 hours post-injection and compared to biopsies of normal (unmanipulated) skin (Figure 1A). The VZV injection site was assessed for clinical score 72 hours after injection and the induration, palpability and change in erythema from baseline were measured and scored, as described before[11]. We showed previously that mononuclear phagocyte numbers were increased at the site of saline injection in old but not young subjects and that this accumulation negatively correlated with the magnitude of antigen-specific responses induced in the contralateral arm of the same individual[9]. Multiparametric flow cytometry on disaggregated skin biopsies from old donors showed no change in the number of $CD11c^+$, $CD1c^+$ or BDCA-3^+ dendritic cells (DC) in response to saline challenge (Extended Data Figure 2A-D). Neutrophils, as determine by CD66b expression by immunofluorescence or $CD45^+lineage^-CD16^+HLA\text{-}DR^-$ by flow cytometry were observed at very low numbers in normal skin which did not significantly change after saline injection (Extended Data Figure 3A and B and 4A and B). These data implies that the increase in mononuclear phagocytes was due to accumulation of monocytes.

To enumerate the changes in monocyte numbers following saline injection we assessed paired samples and expressed data as delta change from normal skin. This was to mitigate against inter-personal variation in the magnitude of responses observed (Extended Data Figure 4A). CD14 was used to identify monocytes in these experiments as it is expressed by the majority of peripheral blood monocytes (classical and intermediate) while $CD16^+CD14^-$

monocytes were relatively rare in the skin (Extended Data Figure 5A). There was a significant increase in $CD14^+$ cells in saline injected skin at 6 hours post-injection (Figure 1B and 1C). We next investigated the expression of CCR2, a chemokine receptor for CCL2, which is highly expressed by $CD14^+$ monocytes[13, 14]. There was a significant increase in number of $CD14^+CCR2^+$ cells in saline injected skin as compared to normal skin in old but not young subjects (Figure 1C, larger images can be seen in Supplementary Figure 1A and B). This response to saline was transient as by 24 hours post-injection similar frequency frequencies of monocytes were detected in normal and saline-injected skin (Extended Data Figure 4B). Multiparametric flow cytometry analysis of normal and saline biopsies, using the gating strategy shown in Extended Data Figure 5A, confirmed that there was a significant increase in $CD14^+$ and $CCR2^+CD14^+$ cells in old saline-injected skin (Figure 1D). We also observed a smaller population of HLA-DR^+ cells that were $CCR2^+CD14^-$ in normal skin, however this population did not significantly change after saline injection (Extended Data Figure 5C). Further phenotyping of the HLA-DR^+ population with CD86, CLA, SLAN, CD16, CX_3CR1 showed that their expression was similar before and after saline injections. The only population that changed in the old subjects after saline-injection were those that expressed CD14 and CCR2, suggesting that it was an increase in the number of $CD14^+CCR2^+$ monocytes rather than a change in their phenotype (Extended Data Figure 5D-F).

To investigate whether this inflammatory response after saline injection in older humans was due to injection with sodium chloride itself or a response to needle injury, we performed intradermal injections with the same volume of air instead of saline (20µl). Air injection also induced a significant increase in the number of monocytes at the site of challenge in old but not young adults compared to normal skin (Extended Data Figure 4C). The accumulation of monocytes was also observed at six hours at the site of VZV injection in old but not young adults (Figure 1E). Taken together these data suggest that old subjects have a heightened inflammatory response to mild skin injury that is not observed in young individuals.

We previously showed that >85% of older individuals have a low VZV response (clinical score between 0-3), while >85% of young individuals have a score of between 3-10[8, 12]. However, a small proportion of older people (~15%) show good cutaneous VZV responsiveness (score above 3), a group we designated as 'old responders'. To assess whether the $CD14^+$ monocyte infiltration was a characteristic of all aged individuals or only those with reduced VZV-specific immunity, we investigated the accumulation of these cells after saline in old VZV responders (red circles) and low responders (filled circles; Fig1F). An increase in monocytes at the site of challenge was only observed in old individuals with a low clinical score while old individuals with a good clinical score behaved similarly to young individuals with low monocyte infiltration. Taken together, there was a significant negative correlation between the fold change in $CD14^+$ monocytes in response to saline challenge and the VZV clinical score (R=-0.38 and p=0.04; Figure 1E), a similar correlation was observed between $CD14^+CCR2^+$ cells and the clinical score (Supplementary Figure 2). Collectively this indicates that the early recruitment of monocytes to the site of skin challenge in old people was associated with decreased antigen-specific immunity.

Senescent stromal cells contribute to recruitment of monocytes in the old.

We hypothesised that the increase in $CD14^+$ cells in the skin was due to recruitment of circulating monocytes, since $CCR2^+$ expression supported the possibility of recruitment in response to CCL2. The alternative explanation that this was a consequence of the proliferation of local tissue-resident macrophages (identified as $CD163^+$), however this was not observed (Extended Data Figure 6A-C). This is in line with murine studies showing dermal macrophages are constantly replenished from the monocyte pool rather than proliferation[15]. We first investigated the activation status of the dermal endothelium to determine whether it was permissive for monocyte recruitment. CD62E, also known as E-selectin, was used as a marker of activated endothelium as it binds to sialylated carbohydrates expressed on leukocytes and facilitates their extravasation into the tissue.

Saline-injected skin of old but not young adults exhibited increased CD62E expression on the $CD31^+$ endothelium when compared to normal skin (Figure 2A and B). Furthermore, transcriptional analysis of skin biopsies indicated that there was increased expression of a range of genes encoding monocyte chemoattractants including *CCL2* (one of the main monocyte chemoattractants), *CXCL10*, *CXCL2* and *CXCL1* in old but not young in response to saline injection (Figure 2C). Increased *CCL2* expression in saline-injected old skin was confirmed by immunofluorescence staining of skin sections (Figure 2D). As expected, there was no significant change in the expression of CCL2 cells in young skin after saline-injection (Figure 2D).

We next examined the source of monocyte chemoattractants and found that resident mononuclear phagocytes were not the main source of CCL2 (Supplementary Figure 9A and B). Using FSP-1 as a marker of fibroblasts, we found that there was a significant increase in the number of fibroblasts expressing CCL2 in the skin of old subjects after saline injection as compared to normal un-injected skin (Figure 2E and F, larger images can be seen in Supplementary Figure 9C). It is known that fibroblasts can produce CCL2[16]. We and others have shown that there are increased numbers of senescent fibroblasts in the skin of older humans[16, 17, 18] and CCL2 is a known component of the senescence associated secretory phenotype (SASP)[19]. Indeed, using p16 as a marker of senescence we found that $FSP1^+p16^+$ fibroblasts were the main source of CCL2 after saline injection of old donors (Figure 2G and H). Senescent fibroblasts made up 54.1% of $CCL2^+FSP1^+$ cells in normal skin which increased to 66.8% in saline-injected skin (Supplementary Figure 9E). Although some non-senescent fibroblast evidently expressed CCL2, our previous data showed that senescent fibroblasts produce significantly more CCL2 than the non-senescent fibroblasts[16]. Therefore, the early production of SASP-related mediators by senescent fibroblasts after saline injection (including CCL2) may lead to the recruitment of inflammatory monocytes to the site of skin challenge. This interaction between senescent cells and monocyte recruitment is supported indirectly by the significant correlation between the number of

senescent fibroblasts present in the skin, as determined by telomere-associated DNA-damage (TAF) foci positive FSP-1+ cells (representative staining can be found in Extended Data Figure 8), present in the skin and the extent of $CD14^+$ monocyte infiltration after saline injection (Fig. 2I, larger images can be seen in Supplementary Figure 9D).

Monocytes inhibit T_{RM} proliferation through production of Prostaglandin E2.

We next investigated the mechanisms by which the recruitment of monocytes reduced antigen-specific immunity in old subjects. We first assessed inhibitory pathways in normal and saline injected skin by RNAseq. We found that saline injection in old individuals increased the expression of a number of immunoglobulin-like transcript (ILT) receptors such as *LILRB3* (ILT5), *LILRB2* (ILT4), *LILRA2* (ILT1), *LILRB4* (ILT3) and *LILRB1* (ILT2), inhibitory ligands such as *CD274* (programme-death ligand 1; PDL-1) and *PDCD1LG2* (PDL-2), ligand for the T cell receptor TIGIT and *PVR*, as well as inducible COX2 enzyme (*PTGS2)* (Figure 3A).

PTGS2 (encoding COX2) was one of the most highly upregulated genes in saline-injected skin of the old subjects[9] and elevated COX2 expression following saline injection was confirmed at the protein level by immunohistology (Figure 3B and C, larger images can be seen in Extended Data Figure 9A). When staining for COX2 was performed in combination with CD14 there was a significant increase in $CD14^+COX2^+$ cells in saline injected as compared to normal skin (Figures 3D). There was no significant difference in the number of $CD14^-COX2^+$ cells (Extended Data Figure 9B), indicating that this increase in COX2 was specific to $CD14^+$ monocytes.

To demonstrate that COX2 expressing monocytes can inhibit the activation of $CD4^+$ T cells, we first induced COX2 expression in monocytes isolated from peripheral blood by stimulation with LPS (1ng/ml) for 3 hours. LPS treatment significantly increased COX2 expression as compared to untreated controls (Supplementary Figure 3)[20, 21]. Unstimulated

and LPS-stimulated monocytes were then co-cultured with autologous peripheral $CD4^+$ T cells in the presence of anti-CD3 and IL-2 and proliferation was assessed after four days. Stimulated monocytes inhibited $CD4^+$ T cell proliferation as compared to control (unstimulated) monocytes (Figure 3E-F). However, production of the cytokines IFNy, IL-2 and IL-10 was not affected at day 4 post-culture. The COX2-specific inhibitor NS-398 was then used to determine if COX2 expression was involved in the inhibition of $CD4^+$ T cell proliferation. Treatment with NS-398 led to a significant increase in the proliferation of the $CD4^+$ T cells (Figure 3G and H and Supplementary Figure 4A). COX2 is involved in the production of a range of lipid mediators, the most common being PGE_2[22]. To establish if PGE_2 was involved in the inhibition of $CD4^+$ T cell proliferation, we blocked the receptor for PGE_2, EP4, on $CD4^+$ T cells using the inhibitor MF-498. Blockade of PGE_2 signalling also significantly increased the proliferation of the $CD4^+$ T cells in the presence of inflammatory monocytes (Figure 3H and I and Supplementary Figure 4B). To confirm that PGE_2 did not alter the monocyte phenotype we cultured monocytes with PGE_2 and assessed their inhibitory receptor (CD112, CD155, Galectin 9, ILT3 and PDL-1, PDL-2) expression and cytokine production. We did not observe any significant effects of PGE_2 treatment on the expression of these receptor in monocytes, confirming that PGE_2 directly affected CD4+ T cells. To assess if the above observations were relevant in the skin of old donors *in vivo*, we investigated Prostaglandin E2 receptor 4 (EP4) expression by skin-resident $CD4^+CD69^+$ T_{RM} cells in older volunteers. (Figure 4A). The majority of $CD4^+$ T_{RM} expressed EP4 (81.2%), indicating that they have the capacity to respond to PGE_2 produced by monocytes. We next assessed the co-localisation of $CD14^+$ monocytes and $CD4^+T_{RM}$ cells in normal and saline injected skin from old subjects. In normal skin, $CD14^+$ monocytes were on average 15.86μm away from $CD4^+$ T_{RM}, however after saline injection the monocytes were significantly closer to the $CD4^+$ T_{RM} (9.47μm; Figure 4B and C). This increased proximity was likely due to increase in the number of monocytes in the skin after saline injection. To confirm that monocytes have the ability to suppress skin $CD4^+$ T_{RM} proliferation, $CD4^+$ T_{RM} were isolated

from the skin using suction blister technology as described previously (Figure 4D)[11]. Skin $CD4^+$ T_{RM} cells were then pre-labelled with CellTrace Violet and stimulated with CD3 and IL-2 in the presence of either stimulated or unstimulated monocytes for four days. We observed a significant reduction in $CD4^+$ T_{RM} cell proliferation in the presence of stimulated as compared to unstimulated monocytes (Figure 4E and F) supporting the hypothesis that $COX2^+$ monocytes have the capability to suppress T_{RM} proliferation.

p38 MAP kinase inhibition significantly reduces CCL2 production from senescent fibroblasts.

We showed previously that treatment of old subjects with the anti-inflammatory p38-MAPK inhibitor, Losmapimod, significantly enhanced the response to VZV antigens in the skin[9]. To investigate if p38-MAPK inhibition altered CCL2 production and inflammatory monocyte recruitment in the skin, RNAseq analysis was performed on biopsies collected from normal skin and from skin 6 hours after saline injection with saline both before and after Losmapimod treatment (study design Figure 5A). We stratified our subjects in the RNAseq analysis according to the extent of clinical score improvement. The individuals that had no improvement in clinical score are represented as white, and those who had the biggest improvement in clinical score after Losmapimod treatment represented by dark green (Figure 5B). A list of all differentially expressed genes can be found in Supplementary Table 4. Saline injection resulted in a large pro-inflammatory response with a significant increase in the expression of inflammatory associated genes such as *CCL2*, *CAFCL8*, *FOSL1*, *IL1B* and *TREM1* at 6 hours pre-Losmapimod treatment (Figure 5C). This response to saline was reduced after Losmapimod pre-treatment (Figure 5C) and of the top six significantly upregulated genes in saline-injected skin as compared to normal were no longer significantly different post-Losmapimod treatment (Extended Data Figure 10A). In addition, there was a strong trend towards reduction in saline-specific gene expression after Losmapimod treatment (p=0.06; Supplementary Figure 14B). RNAseq analysis showed that the

expression of monocyte chemoattractants (induced in response to saline injection) was reduced post-Losmapimod treatment (Extended Data Figure 10E). However, the reduction in genes specific to saline response in old (saline-specific gene expression) did not correlate with improvement in clinical score (Extended Data Figure 10C) and the same was observed with *CCL2* (Extended Data Figure 10D).

After Losmapimod treatment there was a significant reduction in the number of $CCL2^+$ cells and the number of $CCL2^+$ senescent ($p16^+FSP\text{-}1^+$) fibroblasts (Figures 5D, 5E). Treatment of senescent dermal fibroblasts with Losmapimod *in vitro* significantly reduced their CCL2 production, suggesting Losmapimod could have a direct effect on senescent fibroblast *in vivo* (Extended Data Figure 10F). As a result of the reduced CCL2 production, monocyte infiltration in saline injected skin was significantly decreased post-Losmapimod treatment (Figure 5F). A significant reduction in the number of monocytes after Losmapimod treatment was observed when VZV injected skin (6 hour post-injection) was assessed (Figure 5G).

Together, these data indicate that p38-MAPK inhibition significantly reduces CCL2 production from senescent fibroblasts reducing the accumulation of monocytes at sites of saline or VZV antigen challenge in the skin.

p38 MAP kinase inhibition significantly inhibits PGE_2 that restores T cell proliferation.

COX2 expression has been shown to be regulated downstream of p38-MAPK signalling[20, 23], implying that Losmapimod may act by inhibiting COX2 expression *in vivo*. To test this, we performed Western blot analysis of LPS activated monocytes in the presence or absence of Losmapimod. Losmapimod significantly decreased the LPS induced expression of phopho-p38 MAPK and COX2 *in vitro* (Figures 6A and B). In addition, PGE_2 production was also significantly decreased after Losmapimod treatment (Figure 6C). Furthermore, the addition of Losmapimod to co-cultures of $CD4^+$ T cells that were stimulated in the presence of LPS treated monocytes (Figure 6D and E) enhanced their proliferation to a similar extent to that

observed after direct COX2 or EP4 inhibition (Figure 3G and H). In line with these observations, the increase in $CD14^+COX2^+$ cells after saline injection was also inhibited after post-Losmapimod treatment *in vivo* (Figure 6F). These data collectively suggest that *in vivo* Losmapimod can restore $CD4^+$ T cell responses in part through the inhibition of COX2 expression.

p38 MAP kinase inhibition significantly increases T cell infiltration into the site of VZV challenge.

We assessed the clinical score of 42 old subjects after VZV antigen challenge both before and after Losmapimod treatment. We confirmed and extended our previous observations that treatment with Losmapimod significantly increased VZV clinical score (n=42; Figure 7A). No difference was observed between male and female volunteers in their response to Losmapimod treatment (Extended Data Figure 1B). Losmapimod treatment also significantly decreased serum CRP in all individuals, irrespective of whether they showed an improved skin response to VZV challenge (Figure 7B).

We previously identified a significant association between the clinical score after VZV antigen challenge and the accumulation of T cells and DCs at the site of injection[8, 9]. VZV challenged skin sections collected pre- and post-Losmapimod were stained for CD4 or CD8, Ki67 and CD11c (Figure 7C and D). We found that Losmapimod pre-treatment was associated with a significant increase in $CD4^+$ (Figure 7E) and $CD8^+$ (Figure 7G) T cell accumulation in the skin 7 days after VZV injection. The increased number of $CD4^+$ and $CD8^+$ T cells in perivascular infiltrates was associated with an increased proliferation of these cells *in situ* indicated by Ki67 expression (Figures 7F and H)[12]. Concurrently there was also an increase in $CD11c^+$ DCs in the VZV-injected skin post-Losmapimod (Figure 7I), suggesting there was an increase in T cell and DC clusters as observed previously[9]. Taken together our data show that short-term blockade of inflammation using the p38 MAP kinase

inhibitor Losmapimod can significantly enhance the cutaneous immune response to antigen challenge in older adults.

Discussion:

We demonstrate that senescent fibroblasts in the skin of old subjects secrete an array of chemokines including CCL2 in response to tissue injury, such as that induced by injecting saline, VZV or air. This leads to recruitment of inflammatory monocytes into the skin that inhibit skin T_{RM} activation in part by secreting lipid mediators such as PGE_2 via a COX2-dependant pathway. However, short-term systemic p38-MAPK blockade (that also inhibits COX2) leads to a significant reduction in CCL2, infiltrating monocytes and reduced PGE_2 expression in response to injection of saline or VZV antigens. This results in significant improvement of VZV-specific cutaneous T cell responses (Figure 8).

Ageing leads to the accumulation of senescent cells in many tissues including the skin[16, 18]. Therefore the recruitment of inflammatory monocytes by senescent fibroblasts may also contribute to age-related decreased immune responses in other organs. The significant correlation between the number of senescent dermal fibroblasts and the extent of $CD14^+$ monocyte infiltration indirectly supports the interaction between these cells. Although the abundance of senescent cells increases in the skin during ageing[16, 17, 18], there is no overt expression of inflammatory mediators in un-manipulated skin of old subjects[12]. This suggests that at the steady state, the propensity to mount an inflammatory SASP response is inhibited by the increased numbers of $Foxp3^+$ T regulatory cells (Tregs) and PD-1 expressing T_{RM} cells observed in the skin of older people[10, 12]. Thus, the breakdown of homeostasis induced by tissue injury may override pre-existing inhibitory processes.

PGE_2 has disparate roles in immune responses as it has been shown to be pro-inflammatory (causing oedema formation and pain) as well as contributing to resolution of inflammation[22]. PGE_2 can also suppress $CD8^+$ T cells and may delay viral clearance[24]. Here we show that PGE_2 inhibits $CD4^+$ T cell and T_{RM} proliferation *in vitro* thus confirming previous data [25]. Furthermore, PGE_2 has been shown to induce the expansion and increase the function of $Foxp3^+$ Tregs[26, 27] which may explain why these cells increases in the skin during ageing[10, 28].

In addition, PGE_2 may promote immunosuppression by increasing expression of the anti-inflammatory cytokine IL-10 by mononuclear phagocytes[29, 30]. PGE_2 can also have negative effects on DCs[31]. As $CD11c^+$ DCs increase in the skin post-Losmapimod treatment, we cannot rule out that PGE_2 may also have an inhibitory effect on DCs in the skin.

We have confirmed previous observations that monocytes can inhibit antigen-specific responses[32, 33]. This is may be relevant for the Sars-Cov-2 pandemic which disproportionately affects older subjects[34], since inflammatory monocytes have been found in the lungs of patients with severe COVID-19 disease[35] and these cells may inhibit the function of virus-specific T cells, as described above.

Excessive inflammation has been shown to inhibit antigen-specific immunity[36] and reduce vaccination efficacy in many different contexts[37, 38, 39]. In addition to p38-MAPK inhibition, other drugs such as mTOR inhibitors, have been used to enhance immunity after vaccination in older individuals[40]. Furthermore, COX2 inhibitors have shown promise at improving DC-based vaccine efficacy in mouse models of cancer[41]. The data presented here suggests that COX2 inhibitors which are routinely used in other inflammatory conditions could be used to improve immunity in older people. Thus, the inhibition of age associate inflammation in older subjects may be a promising approach for enhancing immunity to infection, cancer therapy and vaccination during ageing.

Acknowledgements:

Funding: This work was funded by the Medical Research Council (MRC) Grand Challenge in Experimental Medicine (MICA) Grant (MR/M003833/1 to ANA, MVS, TF, and NM), MRC New Investigator award (G0901102 to MVS), Dermatrust and MRC responsive mode grant (MR/T030534/1 to ANA), British Skin Foundation (BSF5012 to ANA), Institute Strategic Programme Grant funding from the Biotechnology and Biological Sciences Research Council (BBS/E/D/20002173 to TF and NM) and National Institute for Health Research University College London Hospitals Biomedical Research Centre.

We thank Dr. Iain Laws, Dr. Ruchira Glaser, Dr Lea Sarov-Blat and Dr. Robert Henderson at GSK, Dr Veronique Birault at the Francis Crick Institute and Professor Mahdad Noursadeghi at University College London for support in developing this project. We are also grateful to Glaxo-Smith Kline for providing the drug Losmapimod (MICA agreement with the MRC) and to the Losmapimod team at GSK for organizing the dispatch of the clinical supply of the drug in this Investigator Led study. We would especially like to thank the blood and skin donors who volunteered for this study and to our research nurses Ms Megan Harries-Nee and Ms. Michelle Berkley for their outstanding work

Author contribution:

ESC designed, performed experiments and wrote the manuscript. **MVS** was involved in the overall design of the study, experimental design and wrote the manuscript. **HT** and **OD** performed the experiments. **BBS**, **NM** and **TCF** performed the bioinformatic analysis of the RNA-seq samples. **PS** and **JG** performed clinical procedures and sample collection. **MHR** was the clinical lead for the study and was involved with scientific discussions. **DG** advised experimental design for COX2 and PGE_2 work. **ANA** was involved in the overall design of the study, initiated and coordinated the collaborative interaction between the different research groups, interpreted the data, contributed writing and edited the manuscript.

Competing interests: The authors declare that they have no competing interests related to this work.

References:

1. Gavazzi, G. & Krause, K.H. Ageing and infection. *Lancet Infect Dis* **2**, 659-666 (2002).

2. Diffey, B.L. & Langtry, J.A. Skin cancer incidence and the ageing population. *Br J Dermatol* **153**, 679-680 (2005).

3. Ciabattini, A. *et al.* Vaccination in the elderly: The challenge of immune changes with aging. *Semin Immunol* **40**, 83-94 (2018).

4. Franceschi, C., Garagnani, P., Vitale, G., Capri, M. & Salvioli, S. Inflammaging and 'Garb-aging'. *Trends in endocrinology and metabolism: TEM* **28**, 199-212 (2017).

5. Furman, D. *et al.* Expression of specific inflammasome gene modules stratifies older individuals into two extreme clinical and immunological states. *Nature medicine* **23**, 174-184 (2017).

6. Dinh, K.M. *et al.* Low-grade inflammation is negatively associated with physical Health-Related Quality of Life in healthy individuals: Results from The Danish Blood Donor Study (DBDS). *PLoS One* **14**, e0214468 (2019).

7. Chambers, E.S. & Akbar, A.N. Can blocking inflammation enhance immunity during aging? *J Allergy Clin Immunol* **145**, 1323-1331 (2020).

8. Agius, E. *et al.* Decreased TNF-alpha synthesis by macrophages restricts cutaneous immunosurveillance by memory CD4+ T cells during aging. *The Journal of experimental medicine* **206**, 1929-1940 (2009).

9. Vukmanovic-Stejic, M. *et al.* Enhancement of cutaneous immunity during aging by blocking p38 mitogen-activated protein (MAP) kinase-induced inflammation. *J Allergy Clin Immunol* **142**, 844-856 (2018).

10. Vukmanovic-Stejic, M. *et al.* The kinetics of CD4+Foxp3+ T cell accumulation during a human cutaneous antigen-specific memory response in vivo. *J Clin Invest* **118**, 3639-3650 (2008).

11. Akbar, A.N. *et al.* Investigation of the cutaneous response to recall antigen in humans in vivo. *Clin Exp Immunol* **173**, 163-172 (2013).

12. Vukmanovic-Stejic, M. *et al.* The Characterization of Varicella Zoster Virus-Specific T Cells in Skin and Blood during Aging. *J Invest Dermatol* **135**, 1752-1762 (2015).

13. Patel, A.A. *et al.* The fate and lifespan of human monocyte subsets in steady state and systemic inflammation. *The Journal of experimental medicine* **214**, 1913-1923 (2017).

14. Ziegler-Heitbrock, L. *et al.* Nomenclature of monocytes and dendritic cells in blood. *Blood* **116**, e74-80 (2010).

15. Tamoutounour, S. *et al.* Origins and functional specialization of macrophages and of conventional and monocyte-derived dendritic cells in mouse skin. *Immunity* **39**, 925-938 (2013).

16. Pereira, B.I. *et al.* Senescent cells evade immune clearance via HLA-E-mediated NK and CD8(+) T cell inhibition. *Nat Commun* **10**, 2387 (2019).

17. Dimri, G.P. *et al.* A biomarker that identifies senescent human cells in culture and in aging skin in vivo. *Proc Natl Acad Sci U S A* **92**, 9363-9367 (1995).

18. Ressler, S. *et al.* p16INK4A is a robust in vivo biomarker of cellular aging in human skin. *Aging Cell* **5**, 379-389 (2006).

19. Campisi, J. Aging, cellular senescence, and cancer. *Annu Rev Physiol* **75**, 685-705 (2013).

20. Dean, J.L., Brook, M., Clark, A.R. & Saklatvala, J. p38 mitogen-activated protein kinase regulates cyclooxygenase-2 mRNA stability and transcription in lipopolysaccharide-treated human monocytes. *J Biol Chem* **274**, 264-269 (1999).

21. Mestre, J.R. *et al.* Redundancy in the signaling pathways and promoter elements regulating cyclooxygenase-2 gene expression in endotoxin-treated macrophage/monocytic cells. *J Biol Chem* **276**, 3977-3982 (2001).

22. Kalinski, P. Regulation of immune responses by prostaglandin E2. *Journal of immunology* **188**, 21-28 (2012).

23. Guan, Z., Buckman, S.Y., Pentland, A.P., Templeton, D.J. & Morrison, A.R. Induction of cyclooxygenase-2 by the activated MEKK1 --> SEK1/MKK4 --> p38 mitogen-activated protein kinase pathway. *J Biol Chem* **273**, 12901-12908 (1998).

24. Chen, H. *et al.* Elevated COX2 expression and PGE2 production by downregulation of RXRalpha in senescent macrophages. *Biochem Biophys Res Commun* **440**, 157-162 (2013).

25. Okano, M. *et al.* E prostanoid 2 (EP2)/EP4-mediated suppression of antigen-specific human T-cell responses by prostaglandin E2. *Immunology* **118**, 343-352 (2006).

26. Baratelli, F. *et al.* Prostaglandin E2 induces FOXP3 gene expression and T regulatory cell function in human CD4+ T cells. *Journal of immunology* **175**, 1483-1490 (2005).

27. Sharma, S. *et al.* Tumor cyclooxygenase-2/prostaglandin E2-dependent promotion of FOXP3 expression and CD4+ CD25+ T regulatory cell activities in lung cancer. *Cancer Res* **65**, 5211-5220 (2005).

28. Vukmanovic-Stejic, M. *et al.* Varicella zoster-specific CD4+Foxp3+ T cells accumulate after cutaneous antigen challenge in humans. *Journal of immunology* **190**, 977-986 (2013).

29. Nakanishi, M. & Rosenberg, D.W. Multifaceted roles of PGE2 in inflammation and cancer. *Semin Immunopathol* **35**, 123-137 (2013).

30. MacKenzie, K.F. *et al.* PGE(2) induces macrophage IL-10 production and a regulatory-like phenotype via a protein kinase A-SIK-CRTC3 pathway. *Journal of immunology* **190**, 565-577 (2013).

31. Zelenay, S. *et al.* Cyclooxygenase-Dependent Tumor Growth through Evasion of Immunity. *Cell* **162**, 1257-1270 (2015).

32. Watanabe, R. *et al.* Pyruvate controls the checkpoint inhibitor PD-L1 and suppresses T cell immunity. *J Clin Invest* **127**, 2725-2738 (2017).

33. Sammicheli, S. *et al.* Inflammatory monocytes hinder antiviral B cell responses. *Sci Immunol* **1** (2016).

34. Chen, G. *et al.* Clinical and immunological features of severe and moderate coronavirus disease 2019. *J Clin Invest* (2020).

35. Liao, M. *et al.* Single-cell landscape of bronchoalveolar immune cells in patients with COVID-19. *Nature medicine* (2020).

36. Pence, B.D. *et al.* Relationship between systemic inflammation and delayed-type hypersensitivity response to Candida antigen in older adults. *PLoS One* **7**, e36403 (2012).

37. Fourati, S. *et al.* Pre-vaccination inflammation and B-cell signalling predict age-related hyporesponse to hepatitis B vaccination. *Nat Commun* **7**, 10369 (2016).

38. Muyanja, E. *et al.* Immune activation alters cellular and humoral responses to yellow fever 17D vaccine. *J Clin Invest* **124**, 3147-3158 (2014).

39. Parmigiani, A. *et al.* Impaired antibody response to influenza vaccine in HIV-infected and uninfected aging women is associated with immune activation and inflammation. *PLoS One* **8**, e79816 (2013).

40. Mannick, J.B. *et al.* mTOR inhibition improves immune function in the elderly. *Sci Transl Med* **6**, 268ra179 (2014).

41. Hahn, T. *et al.* Short-term dietary administration of celecoxib enhances the efficacy of tumor lysate-pulsed dendritic cell vaccines in treating murine breast cancer. *Int J Cancer* **118**, 2220-2231 (2006).

Figure legends:

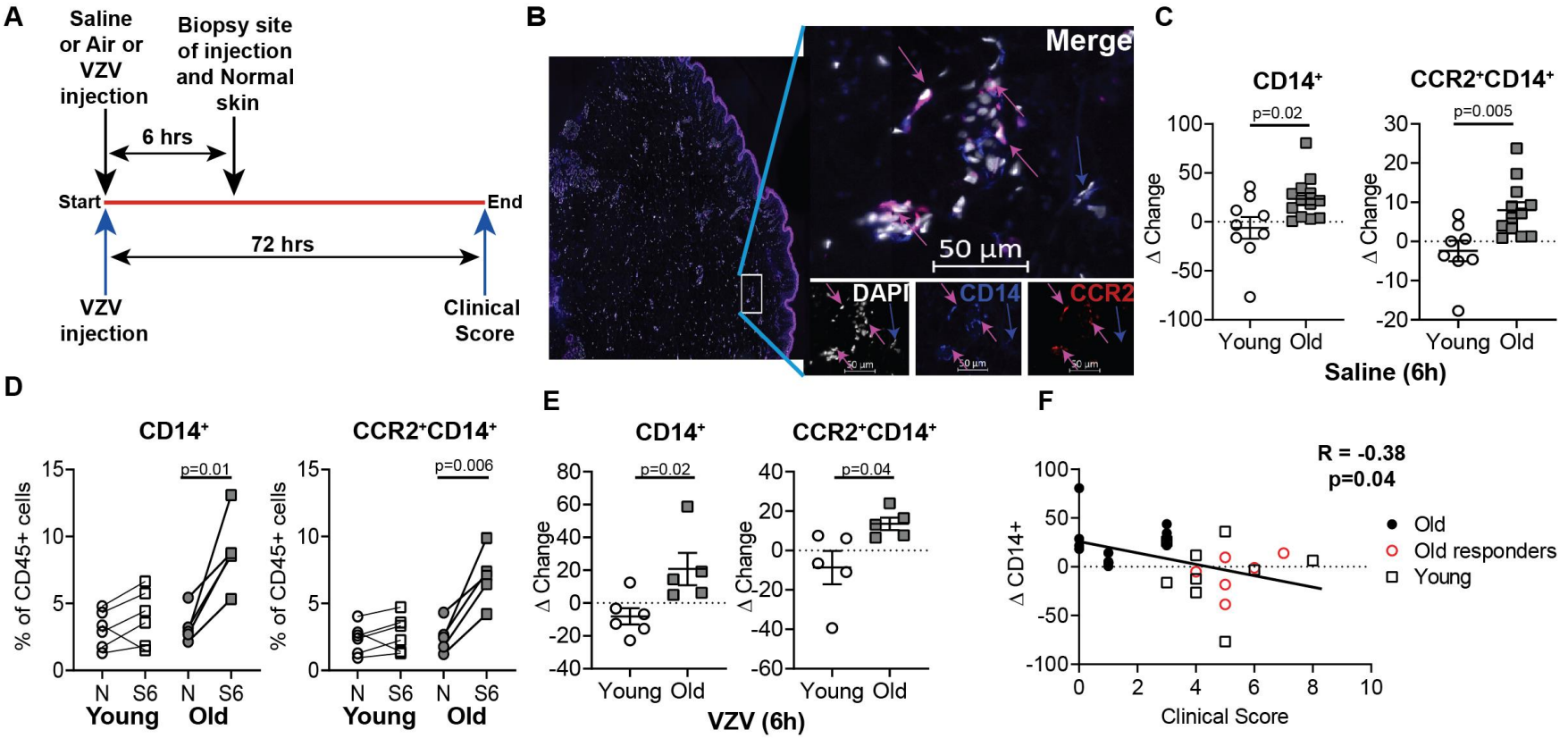

Figure 1: Recruitment of monocytes to sites of injection in the skin

A, Schematic of visits for blood and skin sampling by old (>65 years) and young (<40 years) donors taking part in this study. **B,** representative image of a skin section stained with DAPI (white), CCR2 (red) and CD14 (blue), pink arrows indicate CD14 and CCR2 co-staining and blue arrow indicates CD14 single stain. Cumulative delta change in number of CD14+ or $CCR2^{+}CD14^{+}$ cells in **C,** saline-injected (n=9 young and

n=13 old biologically independent individuals). **D,** cumulative data showing the frequency of monocytes in normal (N) and Saline (6 hours; S6) in skin biopsies collected from young (white; n=6) and old (grey; n=5) individuals as assessed by flow cytometry. Cells were identified as mononuclear phagocytes if they were $CD45^+$Lineage positive but negative for CD3, CD19, CD20 CD56 and $HLA\text{-}DR^+$. The $CD14^+$ and $CD14^+CCR2^+$ cells were assessed as a percentage of CD45+ cells present in the skin. **E,** Cumulative delta change in number of $CD14^+$ or $CCR2^+CD14^+$ cells in VZV-injected skin a (n=5 Young and n=5 old biologically independent individuals) as compared to normal skin. **F,** Correlation between delta change in number of $CD14^+$ cells in the skin after saline injection as compared to normal skin in relation to their VZV clinical response. Old donors are in black filled circles (VZV score 0-3; n=13), Old responders VZV clinical score ≥4; n=6) and young donors (n=9) are in open black square. **C** and **E** shown as mean ± SEM. **C-E** analysed with an unpaired t-test and **F** analysed by Spearmans correlation.

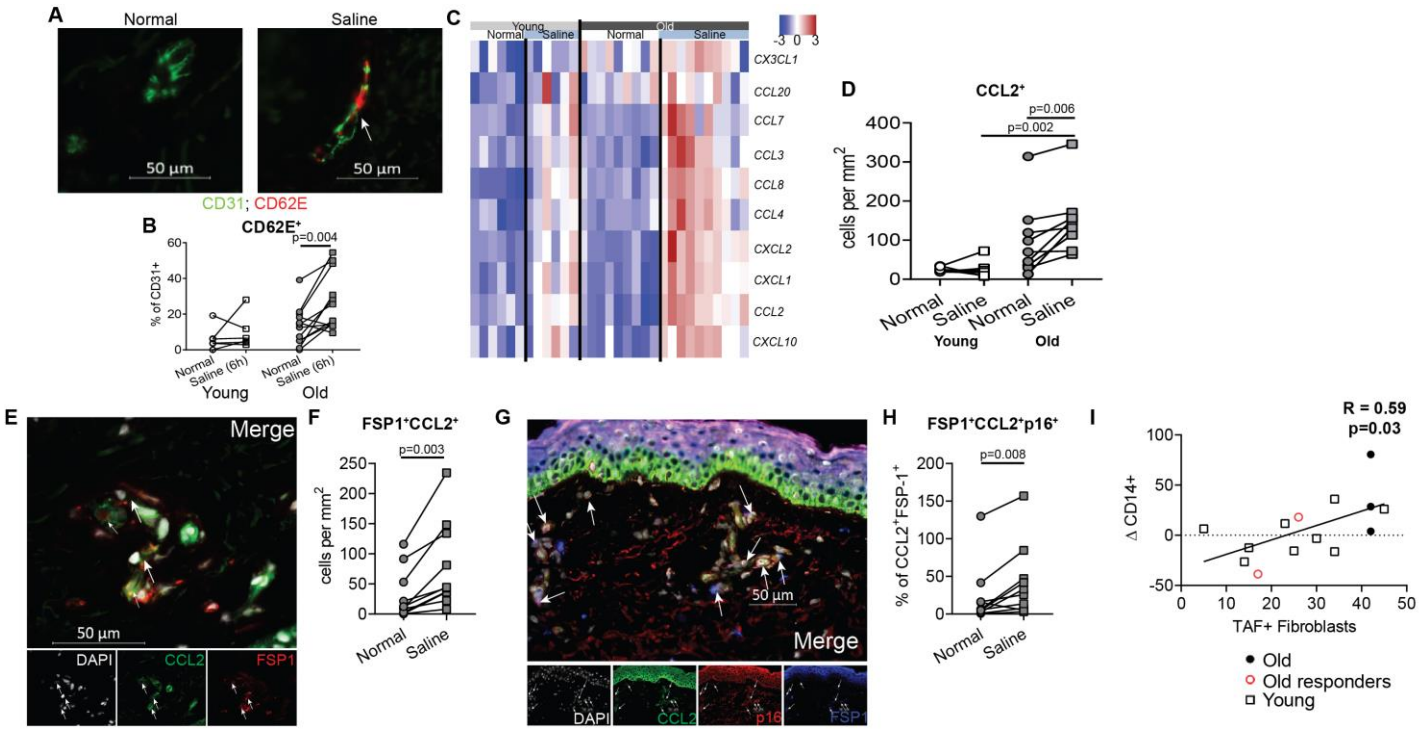

Figure 2: Monocyte chemoattractant expression after saline injection in the skin

A, representative image of normal and saline injected skin stained with CD31 (green) and CD62E (red) and **B,** cumulative data showing the frequency of $CD31^+$ endothelial loops expressing CD62E in young (white; n=6) and old (grey; n=12). **C,** heat map showing expression of monocyte chemokines in normal then saline injected skin of young and old donors and **D,** cumulative data showing number of $CCL2^+$ cells in young (white n=7) and old donors (grey; n=9) and **E,** representative image, arrows indicate double positive cells and **F,** cumulative data showing number of $FSP1^+CCL2^+$ cells in normal and saline injected old skin (n=10). **G,** representative image showing DAPI (white), CCL2 (green), p16 (red) and FSP1 (blue) arrows indicate $FSP1^+CCL2^+p16^+$ cells and **H,** cumulative data of the number of $FSP1^+CCL2^+p16^+$ cells (n=10). **I,** correlation between the number of senescent fibroblast in normal skin (defined as being Telomere associated DNA damage foci [TAF] positive;) and the change in $CD14^+$ monocytes after saline injection in old (black circles; n=3), old responders (red circles; n=2) and young (open squares; n=8) **B, D, F and H,** assessed with a paired t-test and **I,** assessed by a Spearmans rank correlation.

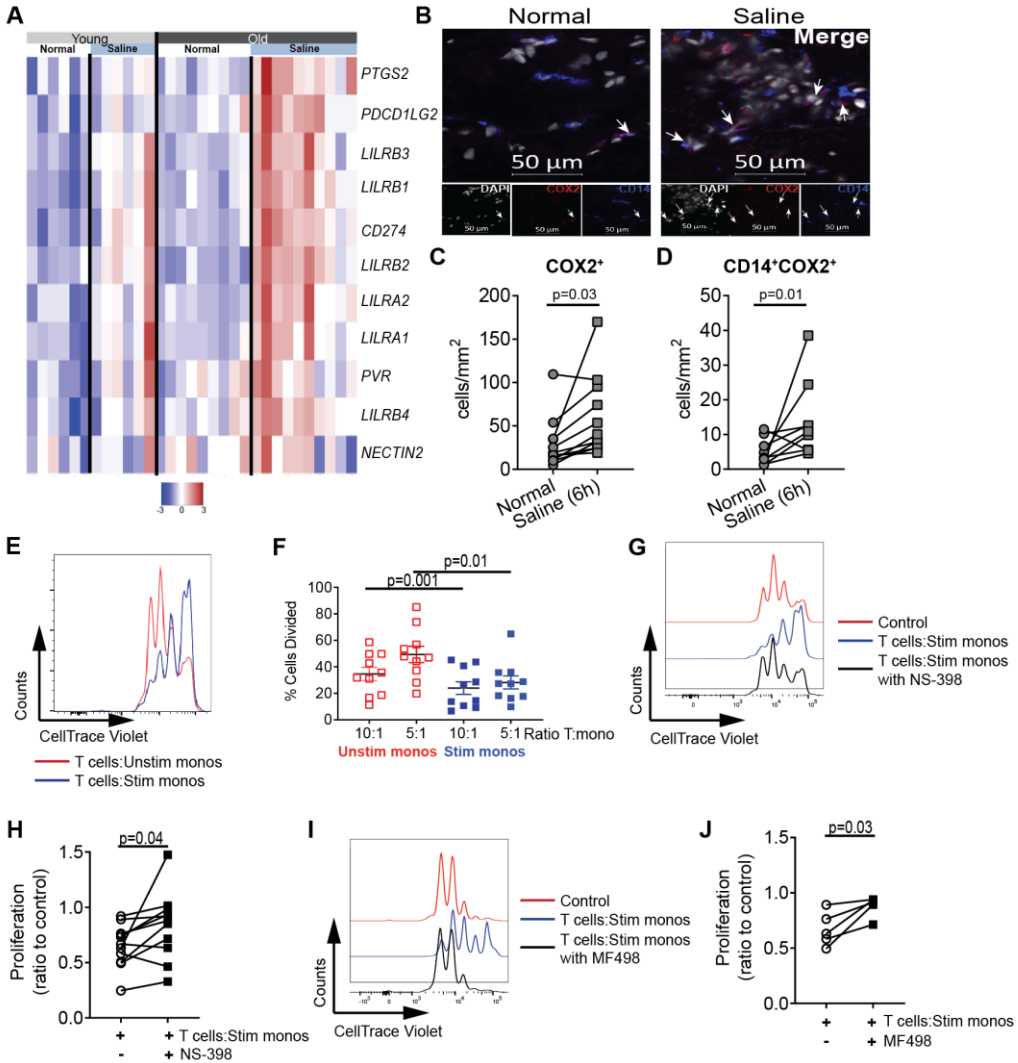

Figure 3: CD14$^+$COX2$^+$ monocytes inhibit T cell proliferation via PGE_2

A, Heatmap showing the expression of genes associated with inhibitory mechanisms in normal and saline injected of old and young donors **B,** representative staining of DAPI (white), COX2 (red) and CD14 (blue) in normal and saline injected skin and **C,** cumulative data of total COX2 expressing cells (n=11) and **D,** number of CD14$^+$COX2$^+$ cells in normal and saline injected skin (n=9). **E**, Monocytes were negatively isolated from the peripheral blood and cultured with and without LPS for 3 hours then subsequently co-cultured with autologous T cells (pre-labelled with CellTrace Violet) that were activated with plate-bound CD3 and IL-2, proliferation was assessed at day 4. A representative flow plot of CellTrace violet dilution in CD4$^+$ T cells co-cultured with unstimulated and stimulated monocytes is shown in **E** and **F,** cumulative data showing percent of cells divided (n=10). A similar co-culture experiment was performed in the presence or absence of the COX2 inhibitor NS-398 (n=11) **G**, and **H,** or the EP4 receptor inhibitor MF498 (n=5) **I,** and **J,.** Control is unstimulated monocytes co-cultured with T cells in the presence of drug. Each data point within each figure is a biologically independent experiment. **F,** shown as mean ± SEM. In **C,D, F, H** and **J** analysed with a paired t-test.

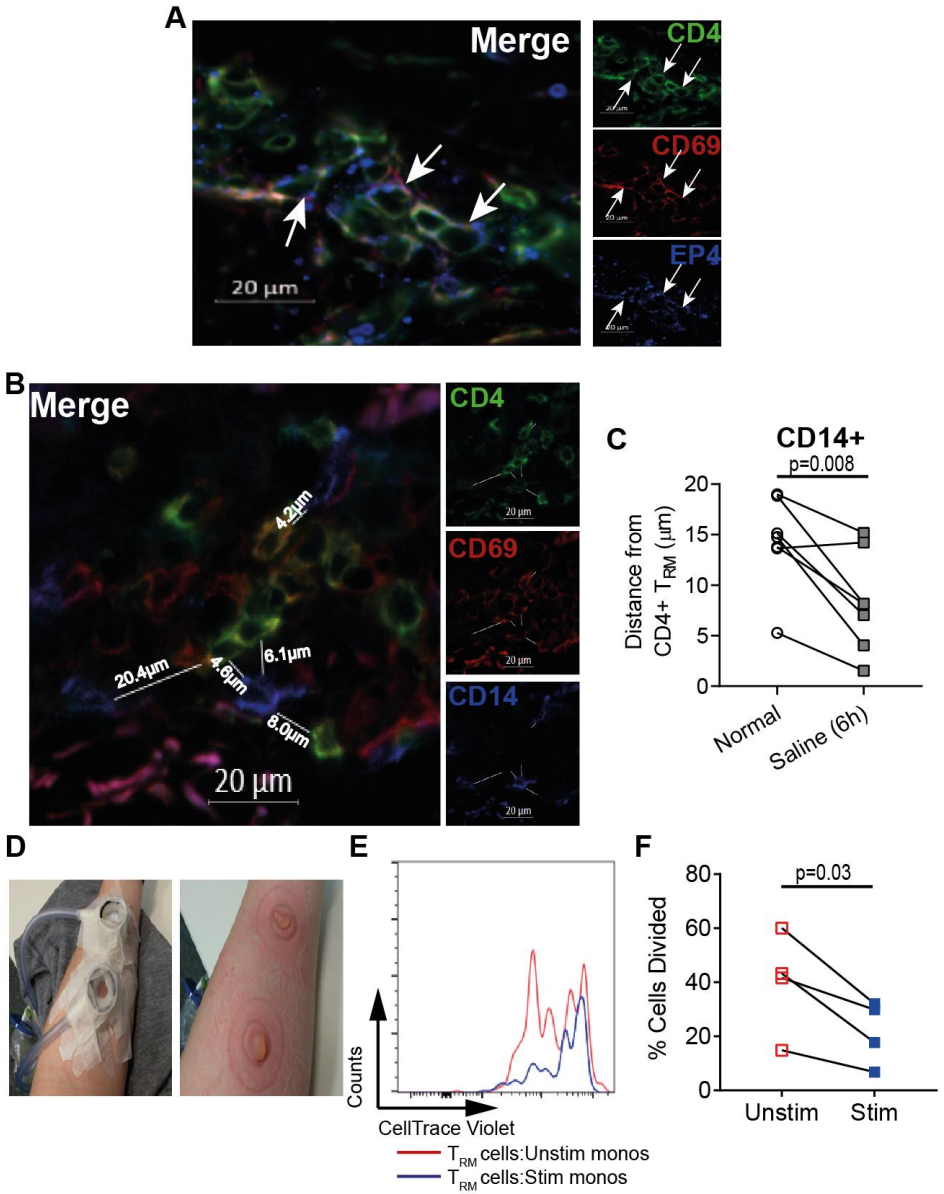

Figure 4: PGE_2 production by monocytes inhibits skin $CD4^+$ T_{RM} cell proliferation.

A, representative staining of CD4 of eight independent donors (green), CD69 (red) and EP4 (blue) in normal skin, white arrows indicate $CD4^+$ T_{RM} cells which co-express EP4. **B,** representative staining showing co-localization of $CD4^+$ T_{RM} cells and $CD14^+$ monocytes (blue) and **C,** cumulative data showing distance of $CD14^+$ monocytes from T_{RM} in normal and saline injected skin from older adults (n=7). Monocytes were negatively isolated from the peripheral blood and cultured with and without LPS for 3 hours then subsequently co-cultured with skin T_{RM} cells (pre-labelled with CellTrace Violet), which were collected from suction blisters (representative image in **D**) then activated with plate-bound CD3 and IL-2 and proliferation was assessed at day 4. **E,** representative flow plot of CellTrace violet dilution in T_{RM} cells co-cultured with unstimulated (red line) or stimulated (blue line) monocytes. **F,** Cumulative data on $CD4^+$ T_{RM} proliferation in the presence of stimulated or unstimulated monocytes, assessed at day 4 (n=4). **C,** and **F,** were analysed with a paired t-test.

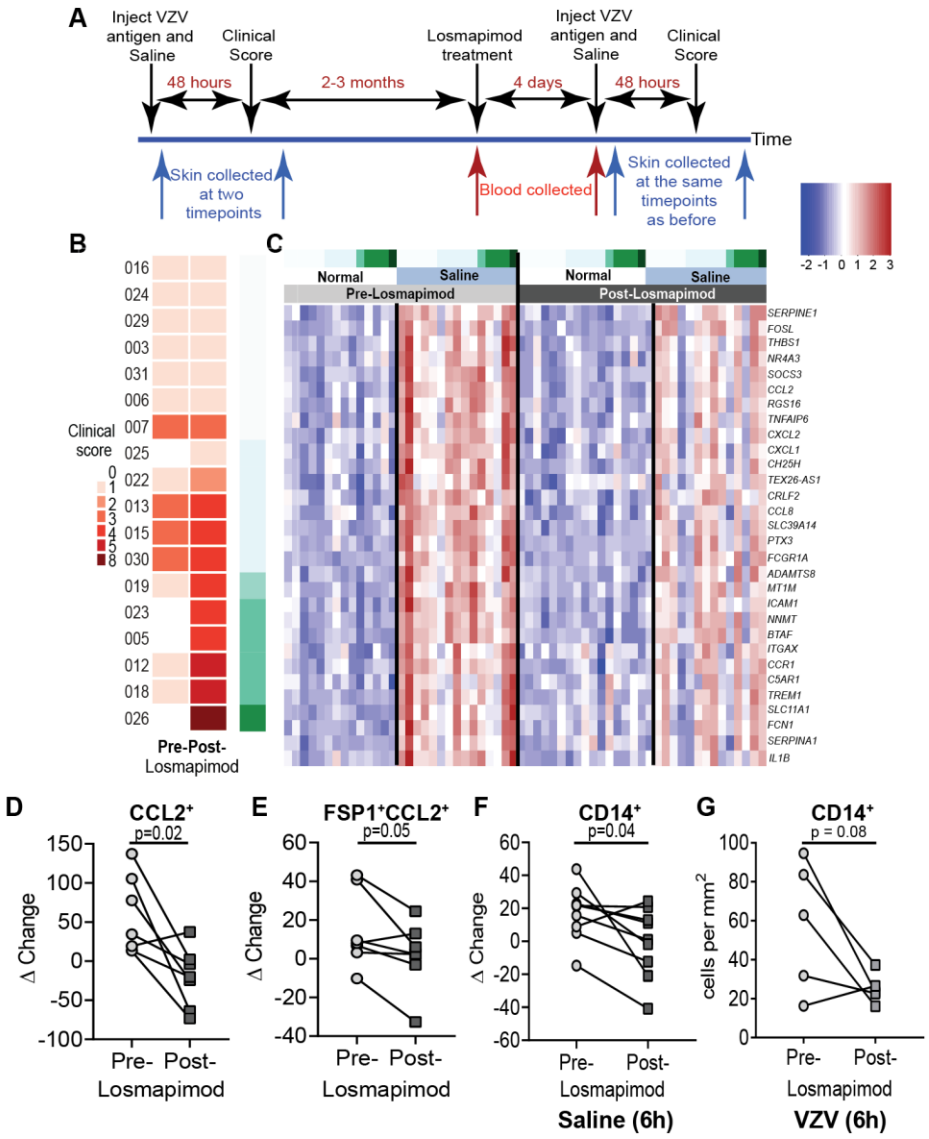

Figure 5: Reduced inflammatory monocyte recruitment to the skin by Losmapimod pre-treatment

A, Losmapimod clinical study diagram. Black arrows indicate study visits, red arrows indicate blood samples collected and blue arrows indicate skin biopsies taken. **B,** Colour coding of the clinical response of each individual after VZV challenge both before and after Losmapimod pre-treatment (pink/brown). Further colour coding was introduced to identify the extent of improvement where dark green identifies the biggest improvement and white shows no improvement in the skin. **C,** This coding was used in conjunction with the transcriptomic signatures in normal and saline injected skin before and after Losmapimod treatment. The top 30 genes upregulated in saline injected skin as compared to normal skin before pre- Losmapimod. **D,** Fold change of $CCL2^+$ cells (n=7 biologically independent individuals) and **E,** % of $FSP1^+CCL2^+$ that express p16 in saline injected pre- and post-Losmapimod treatment (n=7 biologically independent individuals). **F,** fold change $CD14^+$ cell in the skin in response to saline injection (n=9 biologically independent individuals) and **G,** number of $CD14^+$ monocytes in VZV injected skin (6 hours after injection; n=5 biologically independent individuals) pre- and post-Losmapimod treatment. Significance in **D-G** assessed using a paired t-test.

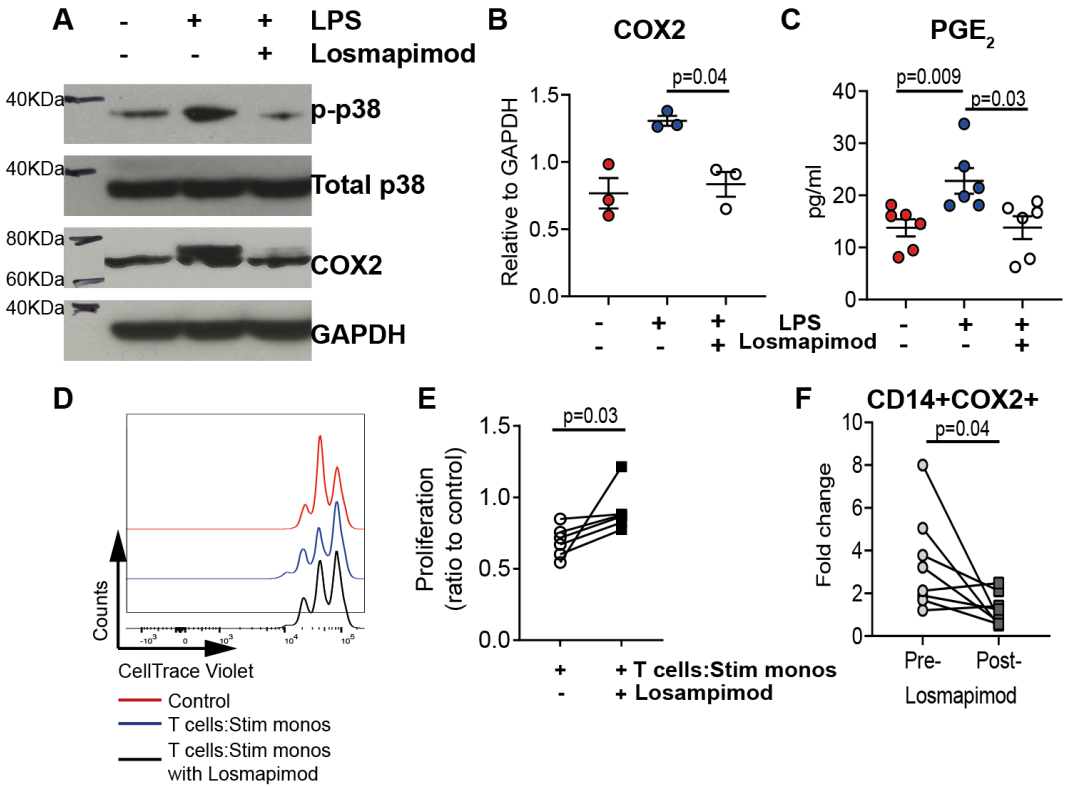

Figure 6: Losmapimod restores T cell function by inhibiting monocyte COX2 and PGE_2 production

Monocytes were negatively isolated from the peripheral blood and cultured with and without LPS and in the presence or absence of Losmapimod for 3 hours, pellets were collected and western blot performed **A,** representative blot of phospho-p38 MAP Kinase (p-p38), total p38 MAP Kinase (p38), COX2 and GAPDH, full scans can be seen as source data fig.6. **B,** cumulative data of COX2 expression assessed by western blot relative to GAPDH (n=3) and **C**, Prostaglandin E2 (PGE_2) production (n=6). Monocytes were negatively isolated from the peripheral blood and stimulated with LPS (blue) and without LPS (red) or with LPS in the presence of Losmapimod (white) for 3 hours then subsequently co-cultured with autologous T cells (pre-labelled with CellTrace Violet) in the presence of plate-bound CD3 and IL-2 proliferation was assessed at day 4. **D,** A representative flow plot of CellTrace violet dilution in CD4+ T cells co-cultured with unstimulated monocytes in the presence of Losmapimod (control; red) or stimulated monocytes (red) or stimulated monocytes in the presence of Losmapimod (black), and **E,** cumulative data showing percent of cells divided (n=6)**. F,** fold change of **i**nfiltration of $CD14^+COX2^+$ cells between normal and saline injected skin before and after Losmapimod treatment (n=8). **B, and C,** shown as mean ± SEM and analysed by a one-way ANOVA with Tukey's multiple comparison test and **E, and F,** analysed with a Wilcoxon matched-pairs signed rank test

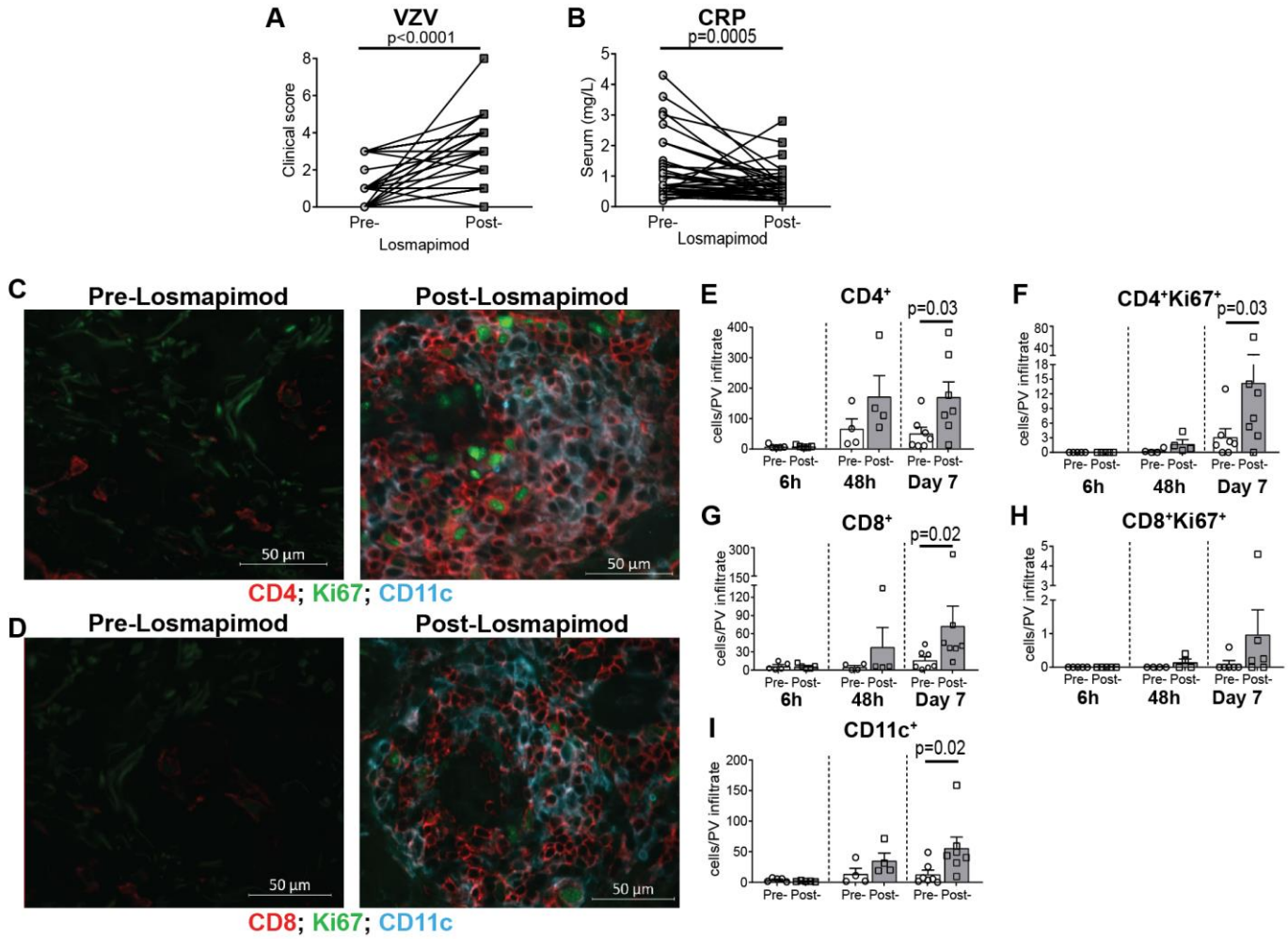

Figure 7: Losmapimod treatment increases VZV induced T cell responses in the skin

A, VZV clinical score and **B**, serum CRP concentrations in all donors pre- and post-Losmapimod treatment (n=42). Representative images of CD11c (blue) and Ki67 (green) and **C,** CD4 (red) or **D,** CD8 (red) staining at 7 days after VZV challenge pre- and post-Losmapimod. Cumulative data of **E,** $CD4^+$ staining, **F,** $CD4^+Ki67^+$ staining, **G,** $CD8^+$ staining, **H,** $CD8^+Ki67^+$ and **I,** $CD11c^+$ staining after VZV challenge in responders pre- and post-Losmapimod. Six hours (6h; n=5), 48 hours (48h; n=4) and Day 7 (n=7). **E-I** shown as mean + SEM and analysed by a wilcoxon-matched pairs test and

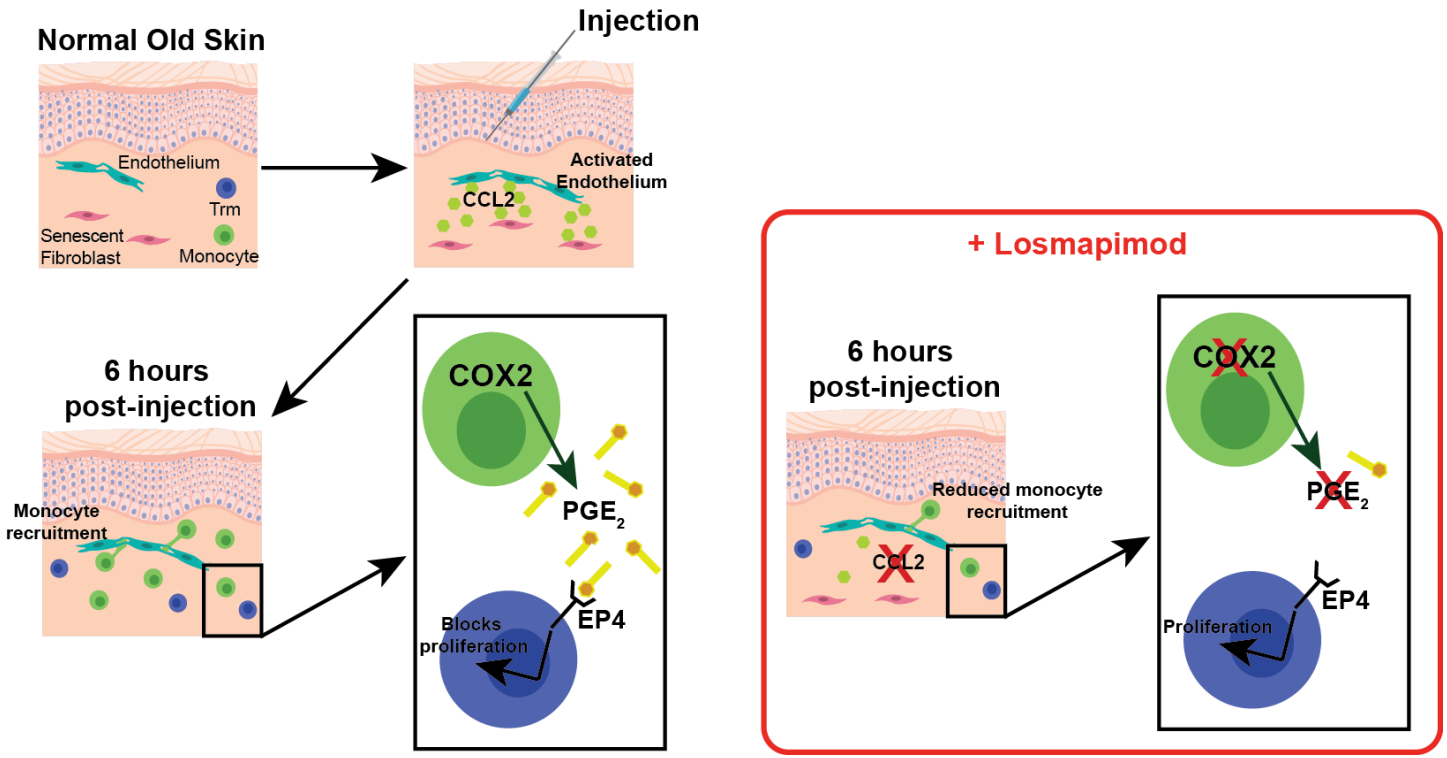

Figure 8: Schematic model of monocyte inhibition of cutaneous immunity in older adults

In older adults the mild damage induced by injection (of air, saline or VZV) results in production of CCL2 from senescent fibroblasts and recruitment of monocytes into the skin 6 hours post injection. The recruited monocytes inhibit T_{RM} proliferation via upregulation of COX2 and subsequent production of the lipid mediator Prostaglandin E2 (PGE_2). The treatment of older adults with the p38 MAPK inhibitor, Losmapimod, results in reduced CCL2 production from the senescent fibroblasts and reduced monocyte infiltration. In addition, p38 MAPK is upstream of COX2 signalling, therefore the treatment with Losmapimod also inhibits COX2 upregulation and reduced PGE_2 production. This significantly increases the T cell response to VZV in the skin of older subjects

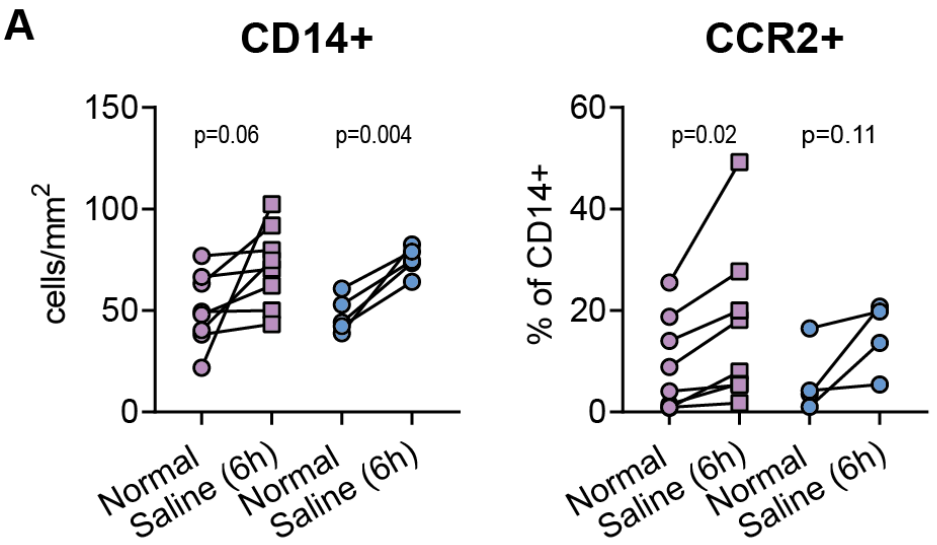

Extended Data Figure 1: No gender difference observed in older adults in response to saline or Losmapimod.

A, cumulative data showing the number of CD14+ and frequency of CCR2+ CD14+ cells in females (pink; n=8) and males (blue; n=5). B, Change in clinical score after Losmapimod treatment in female (pink; n=23) and male (blue; n=19), line indicates median. Data assessed by paired t-test within donor and non-paired t test for comparison between female and males.

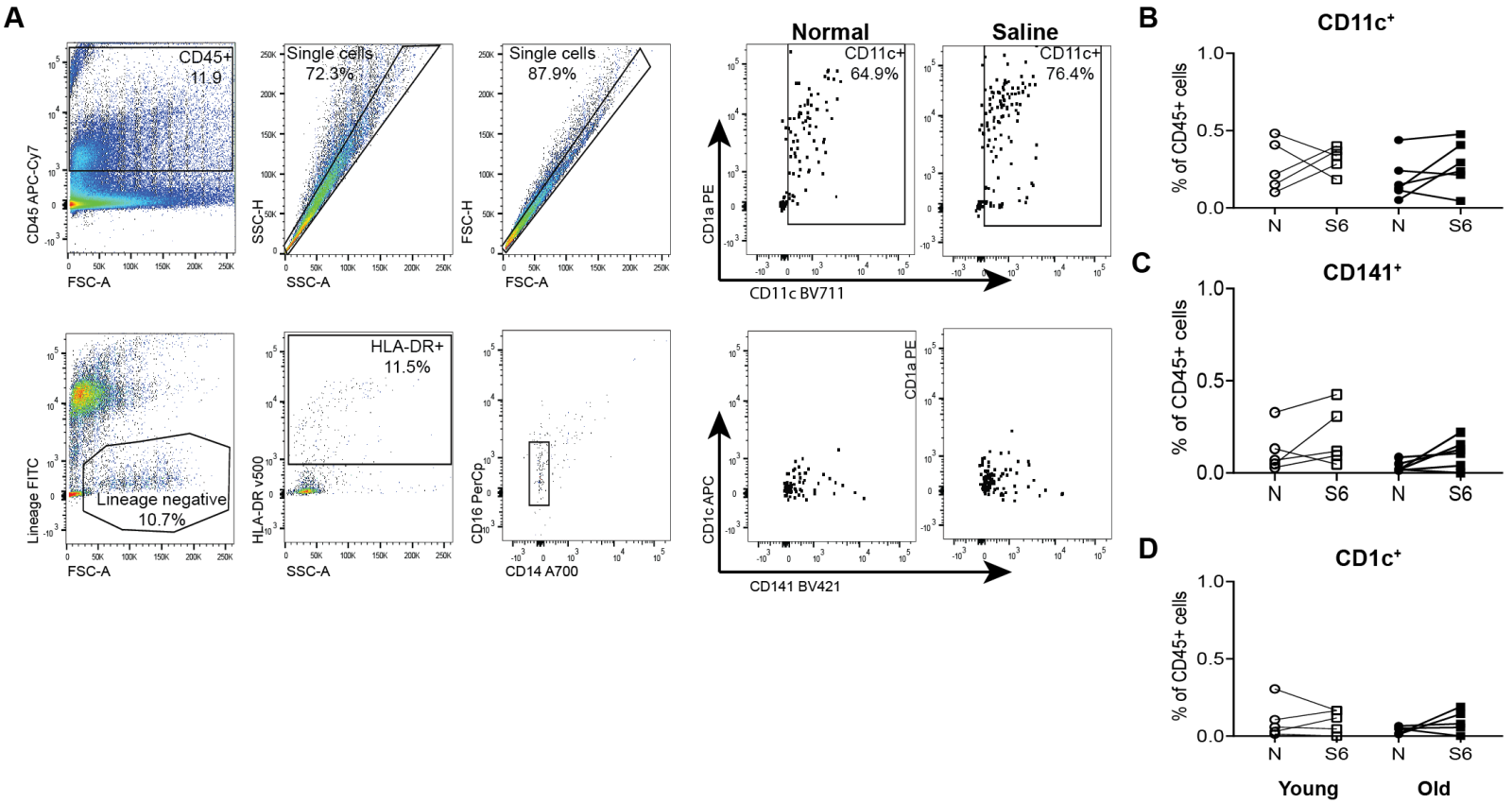

Extended Data Figure 2: Flow cytometric analysis of dendritic cell populations in normal and saline injected skin.

A, Normal and Saline-injected skin were digested overnight and assessed the following day by multiparametric flow cytometry. CD45+ cells were identified, followed by two singlet gates, subsequently cells that were CD3, CD56, CD19, CD20 Zombie Green (Lineage) negative and HLA-DR+ were selected, CD14-CD16-CD11c+ cells were assumed to be dendritic cells. Within the CD11c+ population CD1c and CD141

expression was assessed. Representative staining from Normal and Saline injected (6 hours) skin collected from an older adult is shown. Gating is based upon FMO controls from matched blood sample. Cumulative flow cytometry data of B, CD11c+, C, CD141+ and D, CD1c+ dendritic cells (young n=5; old n=6 biologically independent individuals). Data analysed by paired t test and no significance was found.

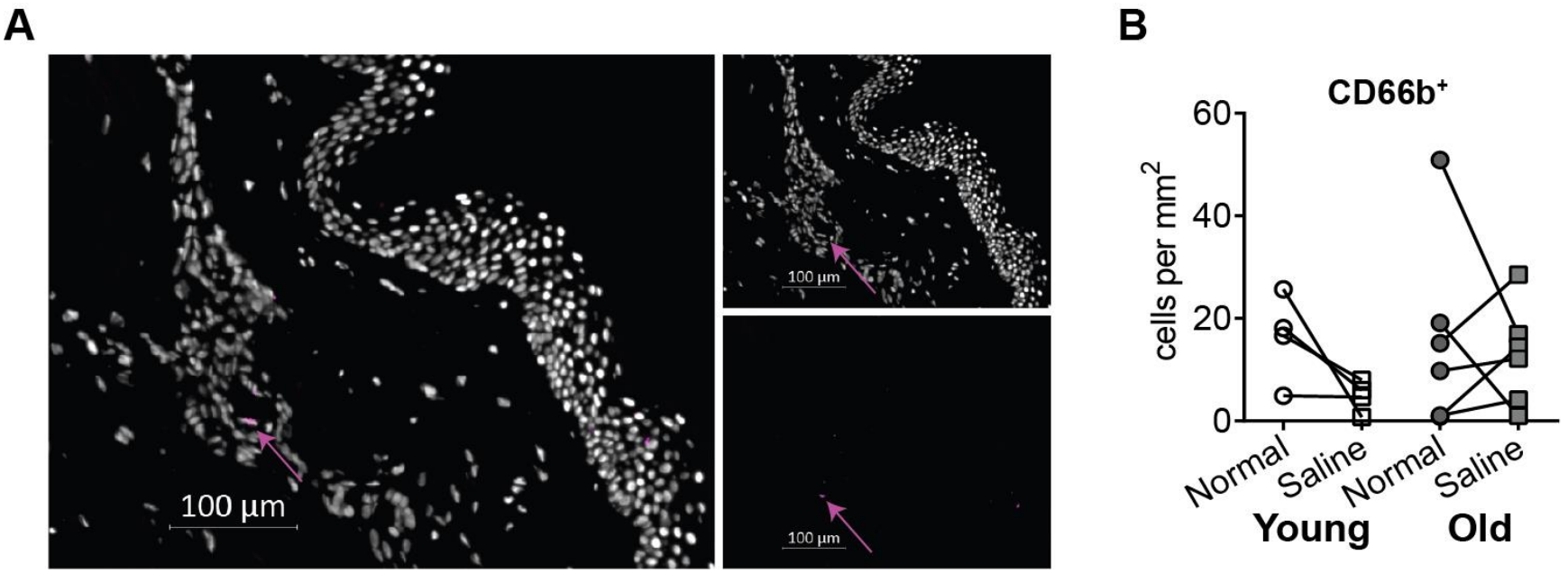

Extended Data Figure 3: No change in CD66b+ neutrophil numbers after saline-injection

A, representative staining of saline-injected skin stained for DAPI (white), and CD66b (purple) and B, cumulative data showing the number of CD66b+ cells in normal and saline-injected young (white) and old (grey) (young n=4; old n=6 biologically independent individuals). Data assessed by paired t-test and no significance was found.

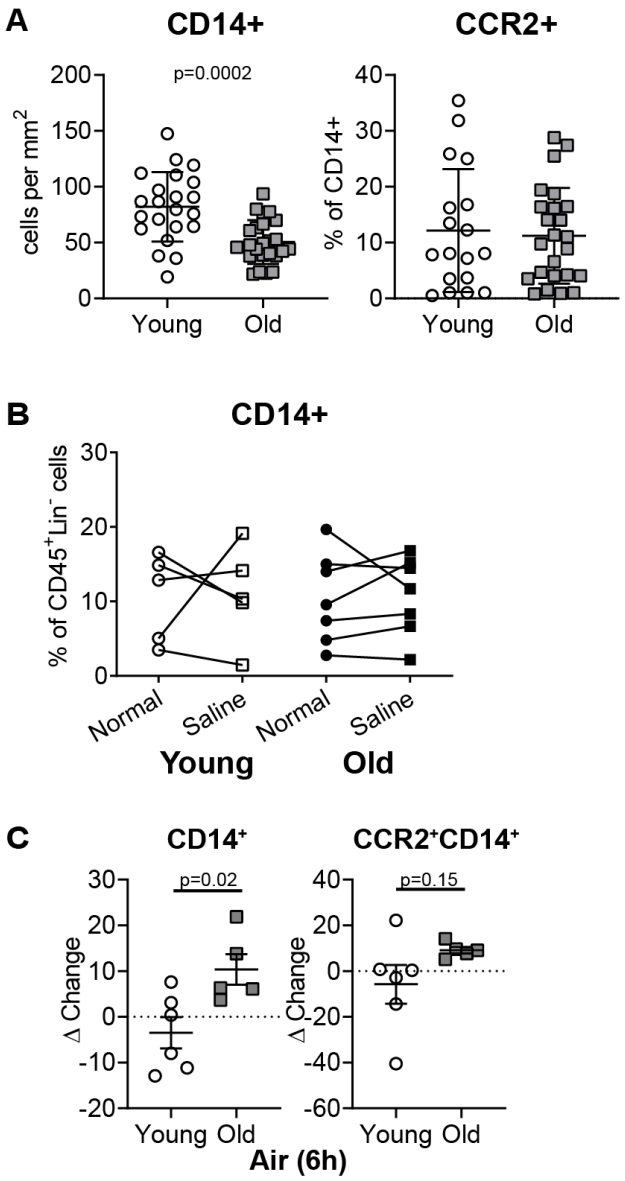

Extended Data Figure 4: Baseline and 24 hours post-saline injection monocyte populations.

A, Comparison of baseline monocyte populations in the skin of based on CD14+ and CCR2+ expression in young (n=22 biologically independent individuals) and old (n=24 biologically independent individuals) individuals . B, Normal and Saline-injected skin were collected 24 hours post-injection from n=5 young (average age 30 years; 3 male and 2 females) and n=7 old (average age 70 years; 2 males and 5 females). Samples were digested overnight and assessed the following day by multiparametric flow cytometry. Cells that were CD45+HLA-DR+and CD3, CD56, CD19 and CD20 negative were considered to be mononuclear phagocytes, within this population CD14+ monocytes were assessed. C, Cumulative delta change in number of CD14+ or CCR2+CD14+ cells in air-injected skin from young (n=6 biologically independent individuals) and old (n=5 biologically independent individuals) volunteers as compared to normal skin. A, and C, shown as mean ± SEM. A and C assessed by an unpaired t test and B, assessed by paired t-test.

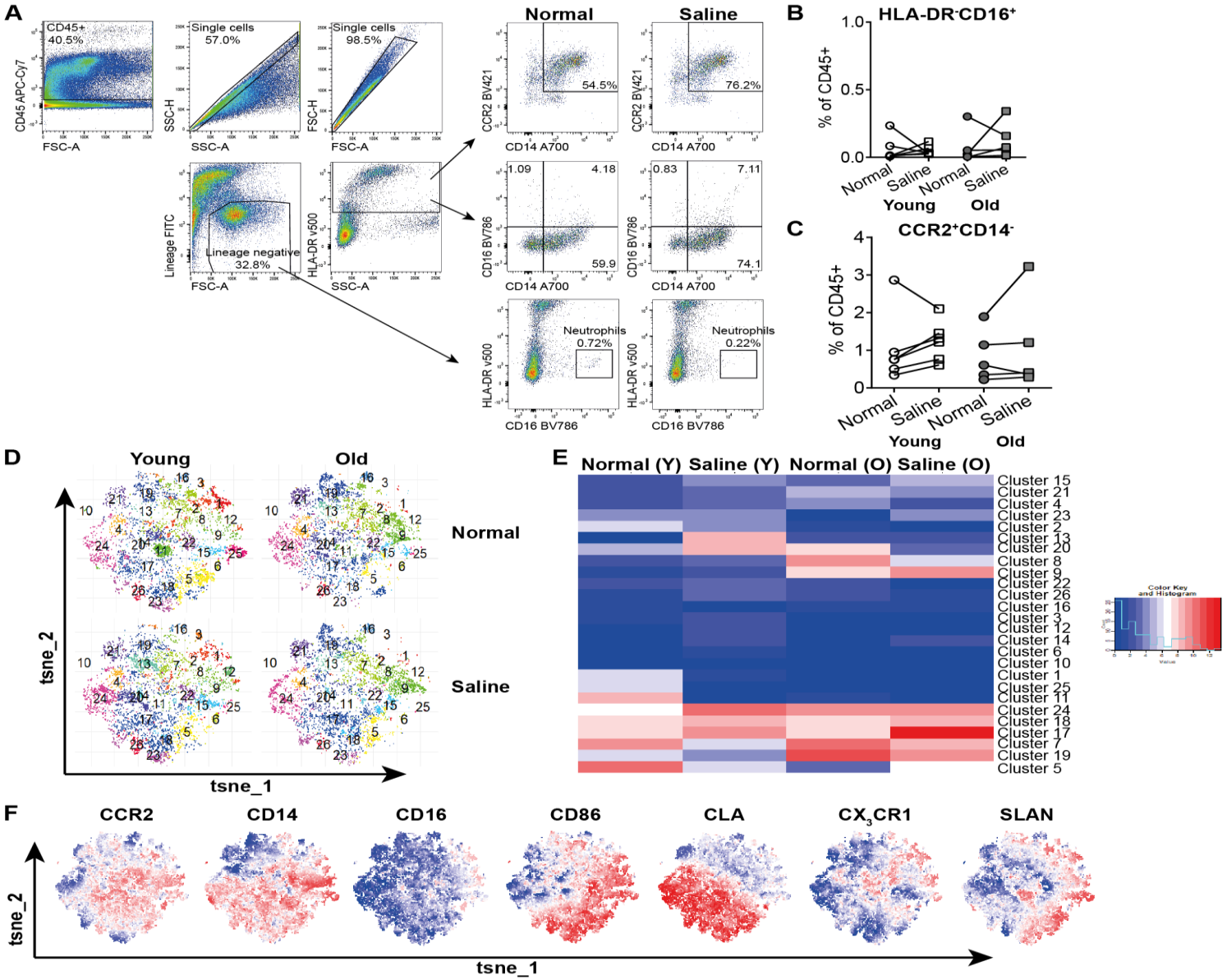
A
CD45+
40.5%
CD45 APC-Cy7
FSC-A
Single cells
57.0%
SSC-H
SSC-A
Single cells
98.5%
FSC-H
FSC-A
Lineage negative
32.8%
Lineage FITC
FSC-A
HLA-DR v500
SSC-A
Normal
Saline
CCR2 BV421
CD14 A700
54.5%
76.2%
CD16 BV786
1.09
4.18
59.9
0.83
7.11
74.1
Neutrophils
0.72%
0.22%
B
HLA-DR-CD16+
% of CD45+
Normal
Saline
Young
Old
C
CCR2+CD14-
D
Young
Old
Normal
Saline
tsne_2
tsne_1
E
Normal (Y)
Saline (Y)
Normal (O)
Saline (O)
Cluster 15
Cluster 21
Cluster 4
Cluster 23
Cluster 2
Cluster 13
Cluster 20
Cluster 8
Cluster 9
Cluster 22
Cluster 26
Cluster 16
Cluster 3
Cluster 12
Cluster 14
Cluster 6
Cluster 10
Cluster 1
Cluster 25
Cluster 11
Cluster 24
Cluster 18
Cluster 17
Cluster 7
Cluster 19
Cluster 5
Color Key and Histogram
F
CCR2
CD14
CD16
CD86
CLA
CX3CR1
SLAN
tsne_2
tsne_1

Extended Data Figure 5: Flow cytometric analysis of monocyte and neutrophil populations in normal and saline injected skin

A, Normal and Saline-injected skin were digested overnight and assessed the following day by multiparametric flow cytometry. CD45+ cells were identified, followed by two singlet gates, subsequently cells that were CD3, CD56, CD19, CD20 Zombie Green (Lineage) negative and HLA-DR+ were considered to be mononuclear phagocytes, within this population CD14+CCR2+ and CD14+CD16+ monocytes and CD16+HLA-DR- neutrophils were assessed. Representative staining from Normal and Saline injected (6 hours) skin collected from an older adult is shown. Gating is based upon FMO controls from matched blood sample. Normal and Saline-injected young (white) and old (grey) skin was assessed by flow cytometry and B, cumulative data of the frequency of CD16+HLA-DR- neutrophils and C, cumulative frequency of the number of CCR2+CD14- cells (young n=7; old n=6). Unbiased representations of multi-parameter flow cytometry data were generated using the t-distributed stochastic neighbor embedding (tsne) algorithmt-SNE. Tsne is a non-linear dimensionality reduction method that optimally places cells with similar expression levels near to each other and cells with dissimilar expression levels further apart. D, tsne cluster plots of young and old normal and saline injected skin and E, heatmap of clusters in normal and saline-injected skin of young (Y) and old (O) adults and F, marker expression plots. Data analysed by paired t test and no significance was found.

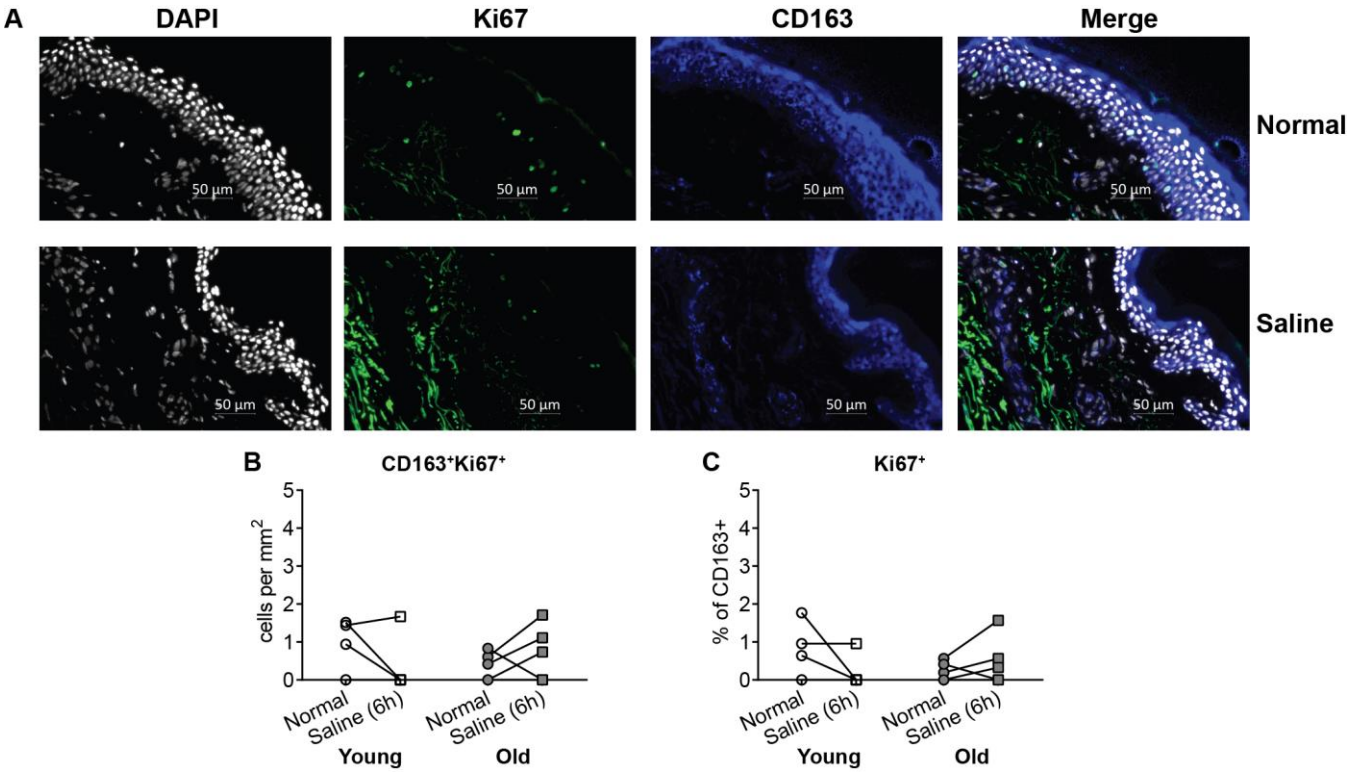

Extended Data Figure 6: Minimal Ki67+ macrophages are observed in saline-injected skin

A, representative staining of normal and saline-injected skin stained for DAPI (white), Ki67 (green), and CD163 (blue) and B, cumulative data showing the number of CD163+Ki67+ and C, frequency of Ki67+ CD163+ cells in young (white; n=4) and old (grey n=5). Data assessed by paired t-test and no significance was found.

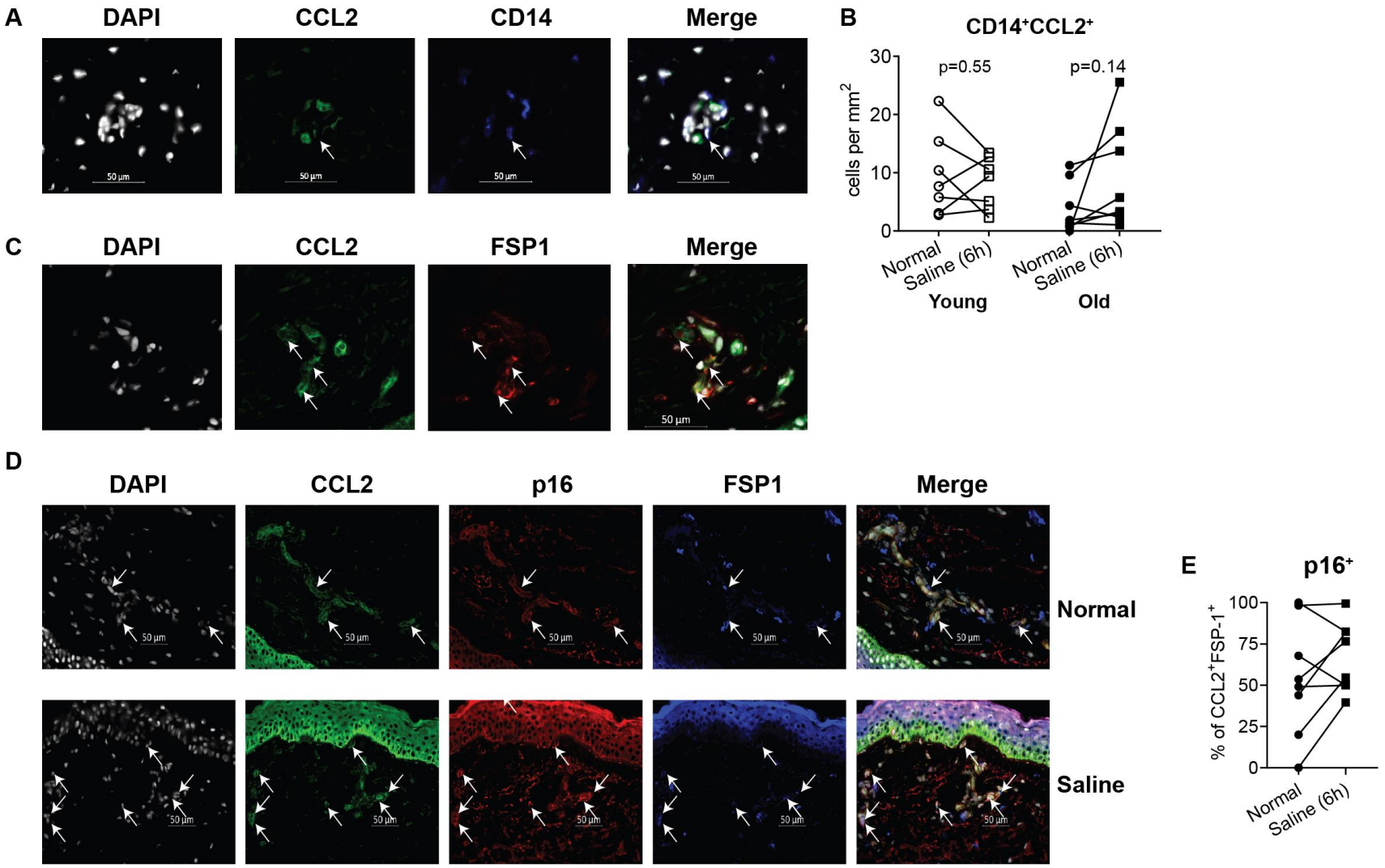

Extended Data Figure 7: Representative staining of monocyte chemoattractant expression after saline injection in the skin

A, representative images of saline-injected old skin stained with DAPI (white), CCL2 (green) and CD14 (blue) and B, cumulative data showing the number of CD14+CCL2+ cells in normal and saline injected skin of young (white n=7 biologically independent individuals) and old skin (black n=8 biologically independent individuals). C, representative staining of saline-injected old skin of DAPI (white) CCL2 (green) and FSP1 (red) and D, representative images of normal and saline-injected old skin stained with DAPI (white), CCL2 (green), p16 (red) and FSP1 (blue). Arrows indicate double positive. E, cumulative data showing the frequency of CCL2+FSP-1+ that express p16+ in old normal and saline-injected skin (n=7 biologically independent individuals). B, and E, assessed with a paired t-test and no significance was found.

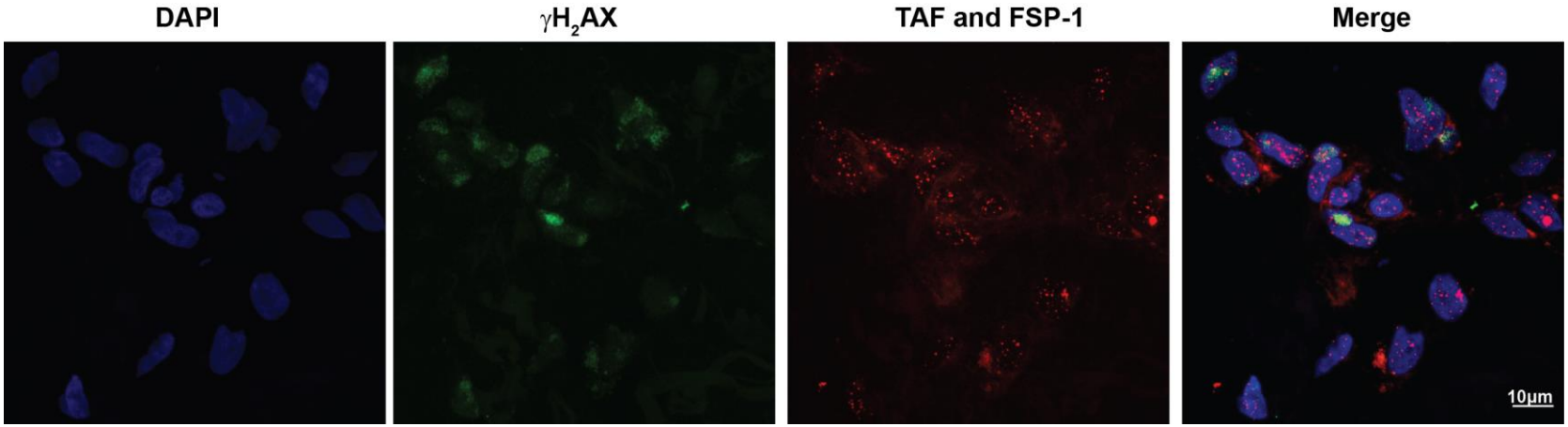

Extended Data Figure 8: Representative TAF staining

Representative images of saline-injected old skin stained with DAPI (white), Telomere probe (intranuclear; red), FSP-1 (cell surface; red), and yH2AX (green).

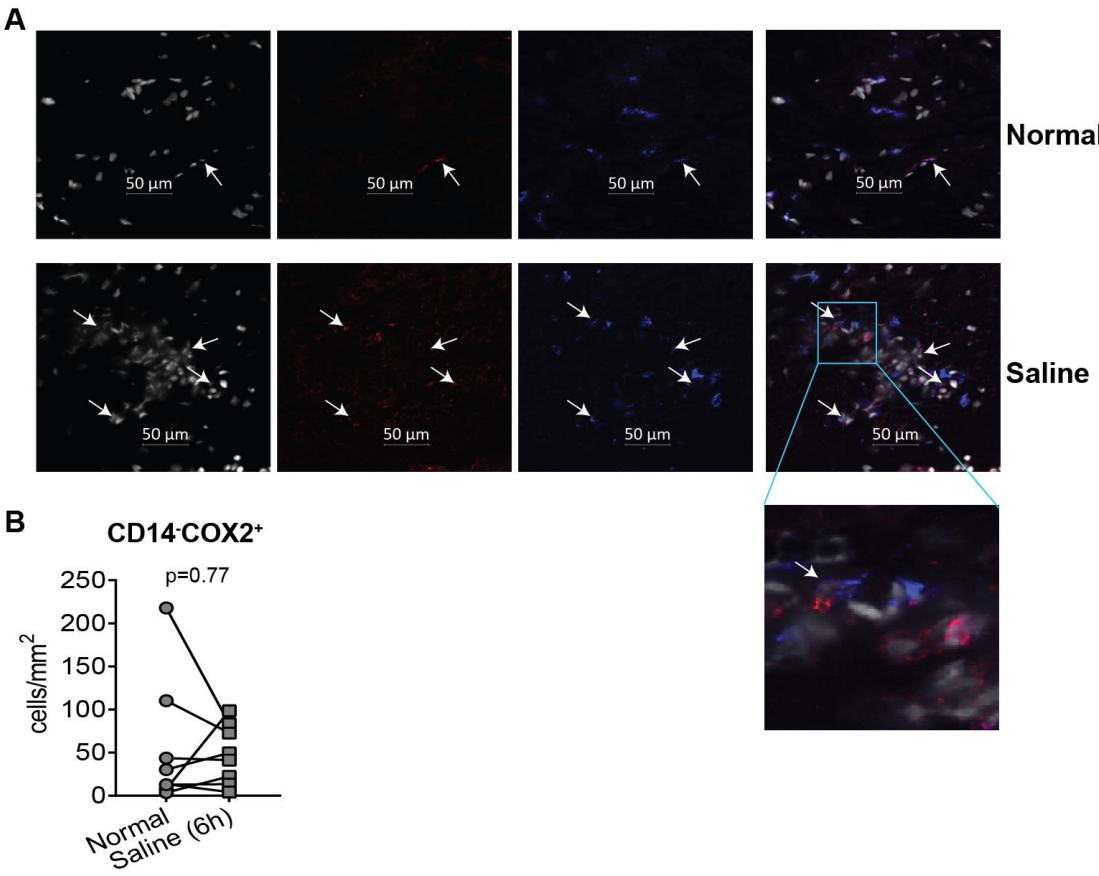

Extended Data Figure 9: CD14 and COX2 staining in normal and saline-injected older skin

Old

A, Representative images of old normal and saline-injected skin sections stained with DAPI (white), COX (red) and CD14 (blue). B, cumulative data showing the number of CD14-COX2+ cells in normal and saline-injected old skin (n= 8 biologically independent individuals).

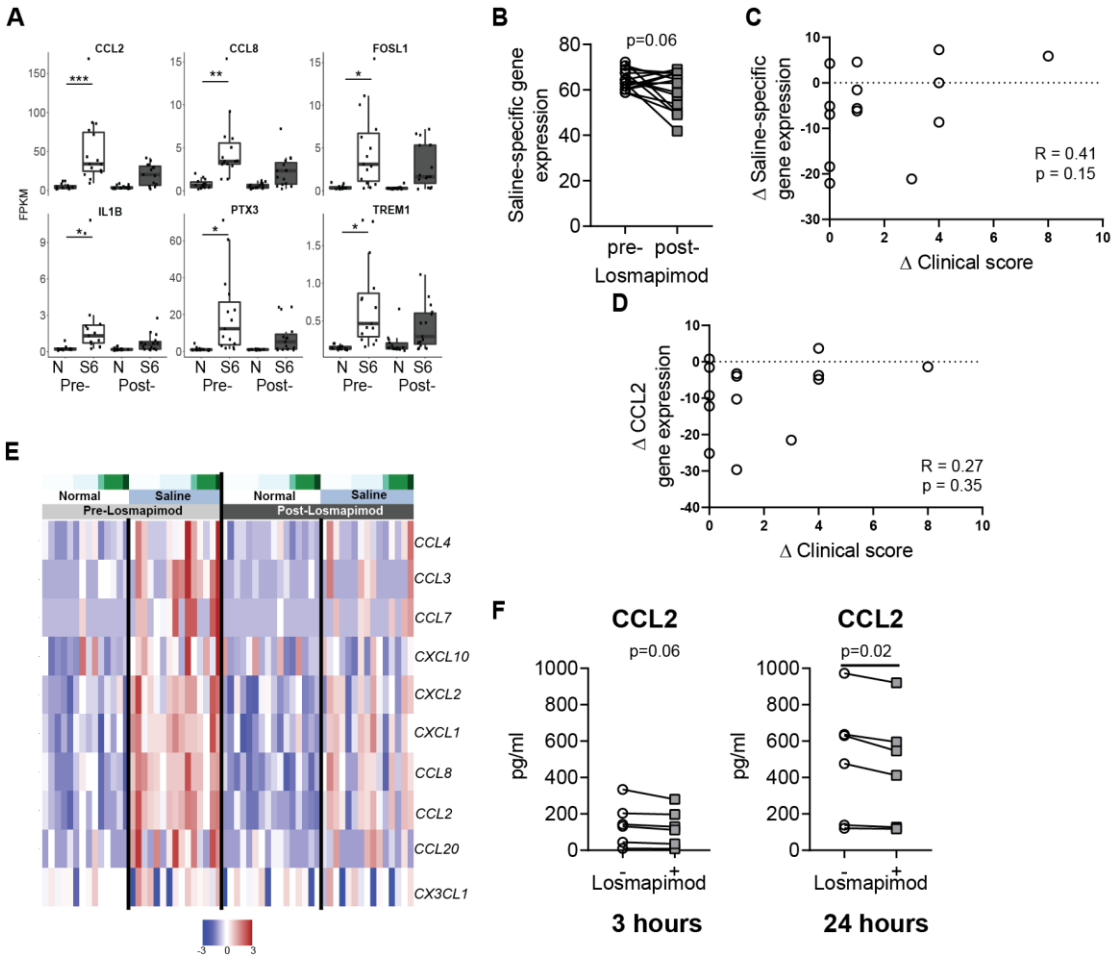

Extended Data Figure 10: Losmapimod reduces the expression of monocyte chemokines

A, top six genes upregulated in saline injected as compared to normal skin, when ranking by average fold change for genes significantly upregulated (adj.p < 0.05) before and after Losmapimod pre-treatment (box shown as median, ± interquartile range and error bars of 1.5*IQR). B, Saline-specific gene expression pre and post-Losmapimod and C, correlation between change in saline-specific gene expression or D, change in CCL2 gene expression and change in clinical score and pre- and post-Losampimod. E, heat map of gene expression of monocyte chemokines in normal and saline injected skin pre- and post-Losmapimod. F, Senescent fibroblasts were cultured with Losmapimod (3μM) for 3 or 24 hours, and supernatants were collected. CCL2 concentrations were assessed by cytometric bead array (n=6). For A-D n=15 biologically independent individuals. B and F assessed by paired t test and C and D assessed by Spearman's rank correlation test. * = p<0.05** = p<0.01 *** = p<0.001

Materials and Methods:

Study design:

The investigation of healthy young (under 40 yrs) and old subjects (65 yrs and over) was approved by the Ethics Committee Queen's Square (London) and by institutional review board (UCL R&D). Individuals with history of neoplasia, immunosuppressive disorders or inflammatory skin disorders were excluded as described in detail elsewhere[9] (see Supplementary Table 1 for donor characteristics). In brief, we excluded individuals with co-morbidities that are associated with significant internal organ or immune dysfunction including heart failure, severe COPD, diabetes mellitus and rheumatoid arthritis and individuals on immunosuppressive regimes for the treatment of autoimmune or chronic inflammatory diseases (e.g. oral glucocorticoids, methotrexate, azathioprine and cyclosporin). In addition, individuals with history of liver disease or elevated liver transaminases (>1.5 times the upper limit of normal), or who had abnormal ECG. All volunteers provided written informed consent and study procedures were performed in accordance with the principles of the declaration of Helsinki. No statistical methods were used to pre-determine sample sizes of this section of our data, but our sample sizes are similar to those reported in previous publications [8, 9, 12, 28].

For the study involving Losmapimod, we recruited 42 healthy older adults (>65 years); 19 males and 23 females with a mean age of 70.7 years old (95% CI 69-72.3 years old). A power calculation was performed to establish effect on change in clinical score, and we assumed an alpha level of 0.05 (2-sided) and a power of 0.90 was considered desirable. VZV skin test was performed and biopsies collected at different time points as described[9]. Only Caucasian European individuals were included in the study and Any individual with a clinical score >3 was excluded from the study as described previously[9]. Two to three months after the first VZV skin challenge the same volunteers received 15 mg Losmapimod (GW856553) twice a day for 4 days (provided by GlaxoSmithKline [GSK] under a Medical Research Council Industrial Collaboration Agreement). We have found previously that the

first VZV challenge did not significantly boost the response to re-challenge of the same individuals after 2-3 months[9]. Losmapimod 15 mg twice a day dose used in this study was chosen on the basis of the PK, PD and safety profiles of Losmapimod observed in GSK Phase I and II studies[42]. These individuals were then re-challenged with VZV skin antigen and biopsies were collected at the same timepoints as before Losmapimod treatment. Clinical scores after VZV injection were performed by two independent researchers and an average reading was recorded. Serum CRP levels were measured with a high sensitivity assay (pre- and post-Losmapimod). No adverse side effects were observed in our study group in response Losmapimod pre-treatment for 4 days.

We were advised by the UK's Medicines and Healthcare products Regulatory Agency (MHRA) that it was not a Clinical Trial of an Investigational Medicinal Product (IMP) as defined by the EU Directive 2001/20/EC. As this experimental medicine study was designed to test a hypothesis in humans *in vivo* and not to determine the therapeutic outcome or efficacy of the drug Losmapimod for patient benefit. Therefore no randomisation was performed. The life sciences reporting summary of this work can be found in the supplementary information.

Skin tests and punch biopsy:

VZV antigen (BIKEN, The Research Foundation for Microbial Diseases of Osaka University, Japan) or 0.9% saline solution or an equal volume of air was injected intradermally into sun unexposed skin of the medial proximal volar forearm as per manufacturer's instructions. Induration, palpability and the change in erythema from baseline were measured and scored on day 2 or 3 as described previously[11]. A clinical score (range 0-10) based on the summation of these parameters was then calculated. Donor characteristics can be found in Supplementary Table 1.

Two punch biopsies (5 mm diameter) were collected from normal (unmanipulated skin) and either saline injected or VZV injected site (at time-points as indicated). Biopsies were frozen in OCT (optimal cutting temperature compound; Bright Instrument Company Ltd). 6µm sections were cut and left to dry overnight and then fixed in ethanol and acetone and stored at -80ºC.

Immunofluorescence:

Sections were stained with optimal dilutions of primary antibodies and followed by relevant secondary antibody conjugated to various fluorochromes as described (Supplementary Table 2). Skin sections were imaged on the AxioScan Z1 slide scanner and analysed using Zen Blue (Zeiss) For normal and 6 hour injected skin and endothelium counts, total cells in the upper dermis were counted and numbers of cells per mm^2 were calculated. Images were taken from the upper dermis, an example of which is shown in Figure 1. For VZV injected skin (days 2-7) the number of cells in five of the largest perivascular infiltrates present in the upper and mid dermis were selected for analysis and an average was calculated as described previously[10]. Staining for telomere-associated ɣH2AX foci (TAF) were carried out as described previously[16]. Counting was performed manually, the data was blinded to the assessor to avoid any bias and where multiple skin sections from one sample were assessed the average of the counts was used.

Skin Biopsy digestion for flow cytometric analysis:

Skin biopsies (5 mm) were taken from normal and saline injected skin (6 or 24-hours post-injection) and disaggregated by overnight incubation (37ºC) in either 0.8 mg/ml collagenase IV (Sigma Aldrich) with 20% FCS or a whole skin digestion kit from Miltenyi Biotec. Single cell suspensions were obtained and subsequently stained with the cell surface antibodies as listed in Supplementary Table 3. Samples were assessed by flow cytometric analysis on a

BD Fortessa using FACSDIVA software, and subsequently analysed using FlowJo Version X (BD Biosciences).

Unbiased representations of multi-parameter flow cytometry data were generated using the t-distributed stochastic neighbour embedding (tsne) algorithm. The R package “Rtsne” available on CRAN (github.com/jkrijthe/Rtsne) was used to perform the Barnes Hut implementation of t-SNE on flow cytometry data. FlowJo software was used to export events of interest (in fcs format) for each sample. After using the Bioconductor “flowCore” R package to import fcs file data and the Logicle transform to scale the data similarly to that displayed in FlowJo, 3000 HLA-DR+ events from each samples analysed in parallel were merged and the relevant fluorescent parameters were used.

RNAseq analysis of skin:

Three 3 mm punch biopsies were collected from each volunteer: VZV injection site at 48 hours post-injection, saline injection site at 6 hours post-injection and normal (un-injected) skin as a control. Biopsies were immediately frozen in RNAlater. Frozen tissue was homogenized, and total RNA was extracted from bulk tissue homogenates using RNeasy Mini Kit (Qiagen). Library preparation for RNAseq was performed using the Kappa Hyperprep kit (Roche Diagnostics) and sequencing was performed by the Pathogens Genomic Unit (UCL) on the Illumina Nextseq 500 (Illumina) using the NextSeq 500/550 High Output 75 cycle kit (Illumina) according to manufacturers’ instructions, giving 15-20 million 41bp paired end reads per sample. Reads were aligned to Genome Reference Consortium Human Build 38 (GRCh38) using Hisat2[43]. Samtools was used to select for reads with paired mates. Transcript assembly was carried out using StringTie[44], with gene-level Fragments per Kilobase of transcript per Million mapped read (FPKM) generated using Ballgown[45]. The RNAseq data has been deposited on Gene Expression Omnibus (Accession Number: GSE130633).

Statistical comparisons were made on gene count estimates generated by StringTie. Genes with low expression (<1 count per million mapped reads in 95% of the samples) or short transcript lengths (<200 nucleotides for the longest transcript) were removed. The count matrix was normalised using the TMM method in edgeR (version 3.22.5)[46], followed by contrast fit with voom in limma (version 3.36.5)[47], treating the subject ID as a blocking variable. Statistically significant differentially expressed genes were with an adjusted p-value of less than 0.05 and expression change of greater than 2-fold up or down, were considered to be statistically significant.

Gene correlation networks (GCN) were constructed and visualised using Graphia Professional (Kajeka Ltd, version 2.1; , https://graphia.app/). Genes without a known HUGO gene nomenclature, or with expression < 1 FPKM for all samples, were removed from the co-expression network analysis. The Markov Cluster Algorithm (MCL) was used to define the network clusters using an inflation value of 2.2. Saline-specific gene expression was generated using the average expression (FPKM) for genes that are significant in

Pre-Losmapimod in saline-injected skin as compared to normal (Fold change>2 and p<0.05). RNAseq data that support the findings of this study have been deposited in NCBI Gene Expression Omnibus accession code GSE130633.

Leukocyte isolation from peripheral blood:

PBMC were isolated by density centrifugation using Ficoll-Paque (Amersham Biosciences). $CD4^+$ T cells were purified by positive selection and monocytes were isolated by negative selection according to the manufacturer's instructions (Miltenyi Biotec).

Monocyte and T cells co-culture:

Monocytes ($1x10^6$/ml) were cultured in the presence of LPS (1ng/ml) and/or NS-398 (1µM) at 37^{o}C with 5% CO_2. Monocytes were collected three hours post incubation and washed

once to remove residual LPS. These cells were pre-incubated with inhibitors NS-398 (1µM) or Losmapimod (3µM) where indicated. $CD4^+$ T cells were labelled with CellTrace Violet (Invitrogen) according to the manufacturer's instructions prior to culture. $CD4^+$ T cells and monocytes (unstimulated or LPS stimulated) were co-cultured at different ratios, in the presence of plate-bound CD3 (1µ/ml) and IL-2 (50IU/ml) and MF-498 (1µM) as indicated (at 37^{o}C with 5% CO_2) for four days.

For experiments involving co-culture of monocytes with skin T_{RM} cells, two suction blisters were formed over uninjected skin, as described previously[11]. Cells were collected from the blister the following day and incubated on plastic for 3 hours, to remove mononuclear phagocytes. Cell suspensions (predominantly $CD4^+$ T cells) were removed and labelled with CellTrace Violet and co-cultured with unstimulated or LPS stimulated monocytes as described above.

T cell proliferation assessment:

Samples were collected on day 4 post-culture and stained for the following: CD3 (UCHT1), CD4 (RPA-T4; BD Biosciences) and Zombie NIR™ Fixable Viability Kit (Biolegend). Samples were assessed by flow cytometric analysis on a BD Fortessa using FACSDIVA software, and subsequently analysed using FlowJo Version X (BD Biosciences).

Western Blot analysis:

Cell pellets were harvested and lysed with RIPA buffer (Sigma-Aldrich) supplemented with protease and phosphatase inhibitors (Cell Signalling) for 30 min on ice. Cell lysates were diluted in SDS sample buffer with reducing agent (NuPage, Life Technologies) and boiled for 5 min at 95 °C. Samples were separated by protein electrophoresis at 120 V for 2 h using 10% Bis-Tris pre-cast gels (NuPage) and transferred overnight at 4°C onto Hybond-P PVDF membranes (GE Healthcare). After blocking in ECL blocking agent (GE Healthcare),

membranes were probed with primary antibodies overnight at 4°C. Primary antibodies used were COX2 (ab15191; Abcam), phospho-p38 MAPK (T180/Y182; 9211), and p38 MAP Kinase (9212), GAPDH (2118; Cell Signalling). The membrane was washed and incubated with HRP-conjugated secondary antibodies (GE Healthcare, 1:4000) for 1 h at room temperature. Antibodies were detected using the ECL detection kit (GE Healthcare). Prior to re-probing with different antibodies, membranes were stripped at room temperature with agitation using Restore stripping buffer (Thermo Scientific). Protein bands were quantified using ImageJ software. The integrated density of each band was normalised to GAPDH using the gel analysis function of ImageJ.

Dermal Fibroblast isolation and culture:

Dermal fibroblasts were isolated and cultured as described previously[16]. Senescence was induced in these cells by exposure to X-ray radiation at a total dose of 10Gy at a rate of 5Gy/min. Irradiated cells were cultured for a further 10-28 days to allow for senescence to develop. Senescence was confirmed by staining for SAβ-galactosidase (Cell signalling). Non-senescent (early passage number 4-10) and senescent fibroblasts were cultured in a 48-well plate at 20×10^4 cells per well in the presence of absence of Losmapimod (3μM), and supernatants were collected at 3 and 24 hours.

Assessment of supernatants:

Cytokine concentration in culture supernatants were assessed by cytometric bead array (CBA) according to the manufacturer's protocol. Samples were analysed using a BD Verse flow cytometer (BD Biosciences). The lower limit of detection for each analyte was 1.5pg/mL. For assessment of PGE_2 production from monocyte cultures with a Prostaglandin E_2 Direct Biotrak Assay was used according to the manufacturers protocol (Fisher scientific).

Statistics:

Statistical analysis was performed using GraphPad Prism version 8.00 (GraphPad Software). Data was assessed for normality and the subsequent appropriate statistical two-sided statistical test was performed as indicated in the legend of each figure.

Code availability statement: Scripts used in the RNA-seq analysis can be found on the GitHub repository at https://github.com/barbarashih/arise_losmapimod

Data availability statement: RNAseq data that support the findings of this work, can be found RNAseq data that support the findings of this study have been deposited in NCBI Gene Expression Omnibus, accession code GSE130633. The rest of the data that support the findings of this study are available as source data.

Methods only references:

42. Watz, H., Barnacle, H., Hartley, B.F. & Chan, R. Efficacy and safety of the p38 MAPK inhibitor losmapimod for patients with chronic obstructive pulmonary disease: a randomised, double-blind, placebo-controlled trial. *Lancet Respir Med* **2**, 63-72 (2014).

43. Kim, D., Langmead, B. & Salzberg, S.L. HISAT: a fast spliced aligner with low memory requirements. *Nat Methods* **12**, 357-360 (2015).

44. Pertea, M. *et al.* StringTie enables improved reconstruction of a transcriptome from RNA-seq reads. *Nat Biotechnol* **33**, 290-295 (2015).

45. Frazee, A.C. *et al.* Ballgown bridges the gap between transcriptome assembly and expression analysis. *Nat Biotechnol* **33**, 243-246 (2015).

46. Robinson, M.D., McCarthy, D.J. & Smyth, G.K. edgeR: a Bioconductor package for differential expression analysis of digital gene expression data. *Bioinformatics* **26**, 139-140 (2010).

47. Ritchie, M.E. *et al.* limma powers differential expression analyses for RNA-sequencing and microarray studies. *Nucleic Acids Res* **43**, e47 (2015).